

# Flow Distribution and Mass Transfer in a Parallel Microchannel Contactor Integrated with Constructal Distributors

**Jun Yue**

Dalian National Laboratory for Clean Energy, Dalian Institute of Chemical Physics, Chinese Academy of Sciences, Dalian 116023, China; and Laboratoire Optimisation de la Conception et Ingénierie de l'Environnement (LOCIE), Université de Savoie, Campus Scientifique, Savoie Technolac, 73376, Le Bourget-Du-Lac Cedex, France

**Raphaël Boichot, Lingai Luo, and Yves Gonthier**

Laboratoire Optimisation de la Conception et Ingénierie de l'Environnement (LOCIE), Université de Savoie, Campus Scientifique, Savoie Technolac, 73376, Le Bourget-Du-Lac Cedex, France

**Guangwen Chen and Quan Yuan**

Dalian National Laboratory for Clean Energy, Dalian Institute of Chemical Physics, Chinese Academy of Sciences, Dalian 116023, China

DOI 10.1002/aic.11991

Published online August 28, 2009 in Wiley InterScience (www.interscience.wiley.com).

*Flow distribution and mass transfer characteristics during CO<sub>2</sub>-water flow through a parallel microchannel contactor integrated with two constructal distributors have been investigated numerically and experimentally. Each distributor comprises a dichotomic tree structure that feeds 16 microchannels with hydraulic diameters of 667 μm. It was found that constructal distributors could ensure a nearly uniform gas-liquid distribution at high gas flow rates where the ideal flow pattern was slug-annular flow. Nevertheless, at small gas flow rates where the ideal flow pattern was slug flow, a significant flow maldistribution occurred primarily due to the lack of large pressure barrier inside each distributor, indicating that dynamic pressure fluctuation in parallel microchannels greatly disturbed an otherwise good flow distribution therein. It was further shown that the present parallel microchannel contactor could realize the desired mass transfer performance previously achieved in one single microchannel under relatively wide operational ranges due to the integration of constructal distributors.* © 2009 American Institute of Chemical Engineers *AICHE J*, 56: 298–317, 2010

*Keywords: microchannel, numbering-up, flow distribution, gas-liquid mass transfer, constructal theory*

## Introduction

In recent years, the chemical industry is undergoing rapid transformation due to the increasing economical and environmental pressures.<sup>1</sup> The future chemical process for the production of commodities and intermediate products is

Correspondence concerning this article should be addressed to G. Chen at gwchen@dicp.ac.cn or L. Luo at lingai.luo@univ-savoie.fr

required to be highly efficient, perfectly safe, and environmentally benign for the chemical industry to survive in the globalization of competition and trade, which has opened great opportunities for microreaction technology.<sup>2</sup> By means of integrating microstructured reactors into a variety of unit operations, microreaction technology is expected to have a plurality of advantages for chemical production such as continuous operational mode, well-defined flow property, enhanced heat and mass transfer, improved chemistry, better process safety, and thus has attracted a growing worldwide interest from academia and industry in the past decade.<sup>3–7</sup> Different types of microstructured reactors have now appeared, among which gas–liquid microreactor constitutes an important part in view of its great potential in many gas–liquid mass transfer operations and chemical reactions of industrial relevance, e.g., CO<sub>2</sub> removal,<sup>8,9</sup> direct fluorination,<sup>10–12</sup> liquid phase oxidation<sup>13,14</sup> and hydrogenation,<sup>15,16</sup> direct synthesis of hydrogen peroxide.<sup>17,18</sup>

One efficient phase contacting mode in gas–liquid microreactors is dispersed-phase contacting,<sup>19</sup> that is, a gas–liquid dispersion is first created at the inlet of a single microchannel and further evolves to certain flow pattern downstream to facilitate mass transfer and chemical reactions therein (this type of microreactor is referred to as microchannel contactor hereafter). Depending on the magnitude of the superficial gas and liquid velocities in such microchannel contactors, various flow patterns including bubbly, slug, slug-annular, annular, and churn flows have been observed.<sup>20–22</sup> At comparatively low superficial gas velocities, slug flow is the dominant flow pattern whereas bubbly flow occurs typically at very small superficial gas velocities and relatively high superficial liquid velocities. Slug-annular and annular flows are present at moderate and high superficial gas velocities, respectively, when the superficial liquid velocity is not very high (e.g., <0.5 m/s). Nevertheless, at sufficiently high superficial liquid velocities, churn flow will be eventually obtained upon further increasing the superficial gas velocity in slug flow. Numerous studies have been conducted so far to investigate mass transfer and reaction properties associated with these flow patterns especially concerning slug, slug-annular, and annular flows in microchannels.<sup>9–14,16,23,24</sup>

An increase in the throughput of microchannel contactors can be realized via the numbering-up approach, i.e., by performing gas–liquid contacting in a multitude of microchannels.<sup>3</sup> However, it is not a trivial thing to keep the desired transport and reaction characteristics previously achieved in one single microchannel during this numbering-up process. One of the important issues that should be well addressed is the design of proper fluid distributors to guarantee uniform two-phase flow distribution among parallel microchannels. Different gas–liquid distributing principles have been conceived toward solving this problem.<sup>12,13,25,26</sup> For example, Chambers et al.<sup>12</sup> constructed a parallel microchannel contactor in which gas and liquid were first introduced into two respective cylindrical reservoirs and were thereby fed to 9 or 30 microchannels through a narrow slit. The volume of the reservoirs was designed to be significantly larger than the sum of the volumes of the slit and all microchannels for uniform annular flow to be possible in each microchannel. This uniform flow seemed to be confirmed by their experimental results of a model direct fluorination reaction using fluorine gas. Haver-

kamp et al.<sup>25</sup> integrated an interdigital micromixer containing alternating pairs of gas-feed and liquid-feed channels just in front of 32 parallel microchannels of 300  $\mu\text{m} \times 100 \mu\text{m}$  cross-section. Each gas/liquid bilayer stream formed in the micromixer was fed into one separate microchannel. To ensure flow equipartition, a large pressure barrier was applied in the micromixer side, that is, the widths of the gas-feed and liquid-feed channels in the micromixer were chosen to be much smaller than those of the subsequent contacting microchannels. But their further hydrodynamic study using nitrogen/isopropanol mixture has revealed that this design is still not capable of ensuring a good two-phase flow distribution among parallel microchannels, as evidenced by the simultaneous coexistence of several flow patterns under the majority of their experiments (e.g., bubbly/slug flow, slug/annular flow). Similar pressure barrier concept was also adopted in the design of de Mas et al.<sup>26</sup> in which auxiliary single-phase gas and liquid channels were arranged between the inlet slit of each phase and parallel microchannels. The dimensions of these auxiliary channels were designed to yield pressure drops that were at least one order of magnitude higher than that across parallel microchannels. With this arrangement, two-phase flow maldistribution could be avoided by preventing crosstalk among parallel microchannels. The fluorescence visualization experiments using nitrogen–ethanol mixture in several contactors of this design comprising 20–60 microchannels have indicated qualitatively that a uniform slug flow distribution was present among all microchannels. The designs exemplified above have provided us valuable insights into the possible structures of fluid distributors suitable for parallel microchannel contactors, but their robustness under wider gas–liquid flow conditions still awaits further examination. Besides, it is also a requisite to gain a thorough understanding on the influence of two-phase flow distribution level offered by such distributors on mass transfer and reaction processes occurring simultaneously in parallel microchannels, and therefore a reliable estimation of the whole system performance in practical operations can be achieved. In a word, basic rules that can guide the numbering-up process of microchannel contactors are still not well established as yet.

Recently, Tondeur and Luo<sup>27</sup> have proposed a new type of distributor named as “constructal distributor” which is composed of multiscale internal channel networks optimized on the basis of a compromise between certain constraints (e.g., minimal viscous dissipation and void volume). As its name suggests, the conception of constructal distributor is based on a quite general theory of multiscale shapes and structures in nature and engineering, called the “constructal theory” developed by Bejan and coworkers<sup>28–30</sup> from 1997 on. In the framework of the constructal theory, the connection from the micro-world all the way to the macroworld can be realized in a clever fashion because of its multiscale optimization methodology,<sup>31</sup> which is exactly one of the challenges faced in the numbering-up process of microreaction systems. Thus, it is envisaged that the integration of constructal distributor into microreaction systems may yield promising results, where some encouraging improvements on single-phase flow uniformity and thermal performance have been reported.<sup>32,33</sup>

This article aims to examine the feasibility of integrating constructal distributor into gas–liquid microreactors. A polymer prototype of the parallel microchannel contactor

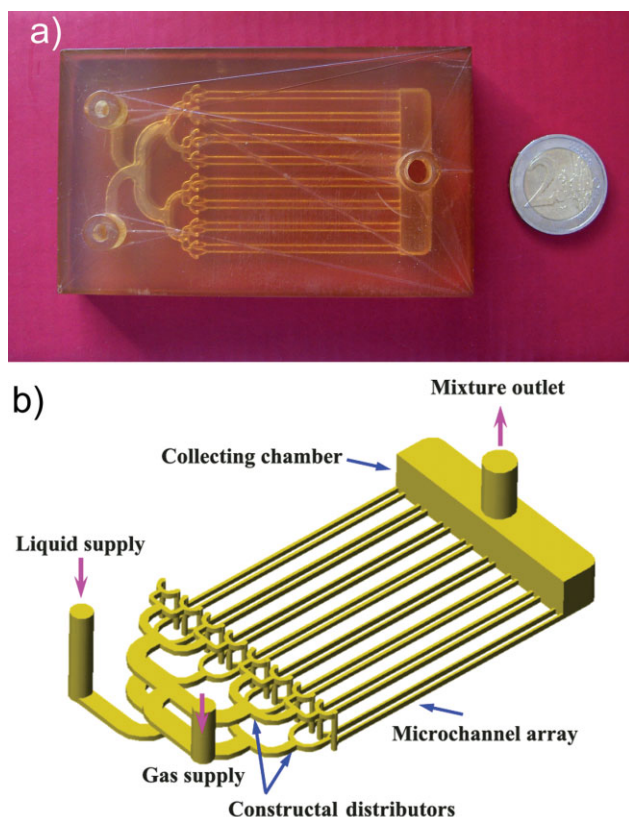


**Figure 1. Parallel microchannel contactor: (a) photo of the contactor and a coin of 2 euro; (b) internal channel structure.**

[Color figure can be viewed in the online issue, which is available at [www.interscience.wiley.com](http://www.interscience.wiley.com).]

integrated in situ with two constructal fluid distributors has been fabricated. Two-phase flow distribution property and the overall mass transfer efficiency in this contactor have been tested in the experiments on physical absorption of CO<sub>2</sub> into water. Numerical simulations are also performed to find out possible factors that will cause two-phase flow non-uniformity in parallel microchannels. Finally, the influence of two-phase flow distribution on mass transfer in parallel microchannels is analyzed, based on which the experimental mass transfer results can be well interpreted.

## Numerical and Experimental Methods

### Description of the parallel microchannel contactor

Figure 1 shows the parallel microchannel contactor used in this study which was fabricated on the photosensitive epoxy resin using laser stereolithography in the “Département de Chimie-Physique des Réactions” located at the ENSIC (Ecole Nationale Supérieure des Industries Chimiques), Nancy, France. The skeleton of the contactor was formed via the stepwise laser-induced polymerization of liquid monolayer, thus generating the desired internal channel structure. More details concerning the fabrication step can be found elsewhere.<sup>27</sup>

The internal channel structure of the parallel microchannel contactor consists of three sections: constructal distributors, the microchannel array, and the collecting chamber, as illus-

trated in Figure 1b. Two flat constructal distributors with dichotomic tree structures have been integrated inside the contactor with the purpose of equally distributing the inlet gas and liquid streams among parallel microchannels. The two distributors are located at planes of different heights to receive the corresponding gas and liquid streams from the single inlet ports on the upper surface of the contactor. The tree structure of both distributors has four generations (Figure 2), where the resulting channels are indexed from 0 to 4 with 0 corresponding to the inlet channel. At the first generation (index 1), the inlet channel is split perpendicularly into two opposing channels. Then each of these channels is further split into another two channels at the second generation (index 2). This bifurcation process continues till the last generation (index 4), finally resulting  $2^4 = 16$  end points at the outlet of each distributor. In contrast to the original design of Tondeur and Luo,<sup>27</sup> a slight structure variation in the current distributors has been made due to different geometric constraints imposed. Firstly, most of the resulting channels are curved instead of straight in order to arrange all the end points at the last generation in the same baseline. At lower generations (gas side: indexes 0–4; liquid side: indexes 0–3), the direction of channels changes smoothly from horizontal to vertical, where the transition regions are connected using circular arcs of 90° (termed as “elbow”). Secondly, the endpoints at the last generation in the gas side (index 4) are downcomers which descend into the plane where the liquid distributor locates (Figure 1b). Then the downcomers are further joined with 16 short side channels of gas downstream in this plane before they meet

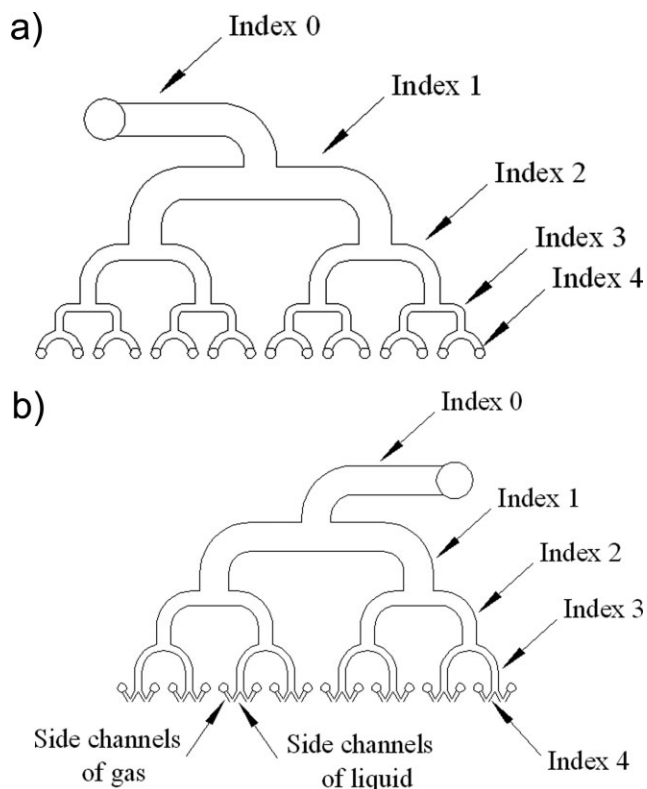


**Figure 2. Channel arrangement in constructal distributors: (a) gas side; (b) liquid side.**

**Table 1. Dimensions of Constructal Distributors**

Distributor	Index	Channel			
		Number	Width (mm)	Depth (mm)	Length (mm)*
Gas side	0	1	3.2	1	23.2
	1	2	3.2	1	21.7
	2	4	1.6	1	14.3
	3	8	0.8	1	6.7
	4	16 <sup>†</sup>	0.8	1	5.7
			16 (downcomers)	Circular, 0.8 mm inner diameter	8
Liquid side	0	1	3.2	1	23.2
	1	2	3.2	1	21.7
	2	4	1.6	1	14.3
	3	8	0.8	1	10.8
	4	16 (side channels)	0.4	1	1
			16 (side channels)	0.4	1

\*For curved channels, the length is calculated as the sum of horizontal, transition, and vertical sections.

<sup>†</sup>Refers to the firstly generated 16 channels shown in Figure 2a.

the corresponding side channels of liquid emerged at the last generation in the liquid side (index 4). The angle between the side channels of gas and liquid is 60°. The detailed dimensions of the two distributors are specified in Table 1. Through the two distributors, the inlet gas and liquid streams are both divided into 16 substreams which are then guided into the microchannel array in order for gas–liquid contacting to occur. In more detail, each gas/liquid stream pair from the respective side channels is thereby fed to one microchannel with hydraulic diameter of 667  $\mu\text{m}$  (rectangular cross-section, 500  $\mu\text{m}$  in width, 1000  $\mu\text{m}$  in depth, and 4.8 cm in length), thus forming a Y-shaped junction inlet geometry. Two-phase mixture from each of 16 microchannels is collected in a nearly cuboid chamber (8 mm  $\times$  8 mm  $\times$  41.5 mm) before flowing out of the contactor.

### Numerical analysis of single-phase flow in constructal distributors

For the parallel microchannel contactor described herein, it may be taken for granted at a first glance that the flow rates of all gas or liquid substreams at the 16 outlet ports of each constructal distributor should be identical in view of the fact that the inlet flow is bifurcated by successive generations with symmetrical tree-like networks (Figure 2). For a better understanding of to what extent this ideality is satisfied, computational fluid dynamics (CFD) has been used to investigate CO<sub>2</sub> and water flows in the respective distributors under ambient condition (20°C). A commercial software, Fluent, version 6.2.16, of ANSYS, Inc., USA, was used here. The computational domain considered in the simulations for each distributor is illustrated in Figure 3. To reduce the calculation work, the simulations were only performed from the inlet channel till the end of the resulting 16 outlet channels right at the beginning of the last generation (index 4) for the gas side and from the inlet channel till the end of the resulting eight outlet channels at the third generation (index 3) for the liquid side. The meshing of the computational domain was made under the software Gambit using tetrahedral elements. Then Navier-Stokes equations were solved in 3D either by a laminar or a turbulent RNG *k- $\epsilon$*  segregated solver based on the following boundary conditions: (1) constant velocity profile normal to the entry face at the inlet port; (2) zero relative pressure condition at the outlet

ports (i.e., two-phase flow in parallel microchannels thereafter was not considered); (3) no-slip condition at the wall surface. For the liquid side distributor, the simulations were

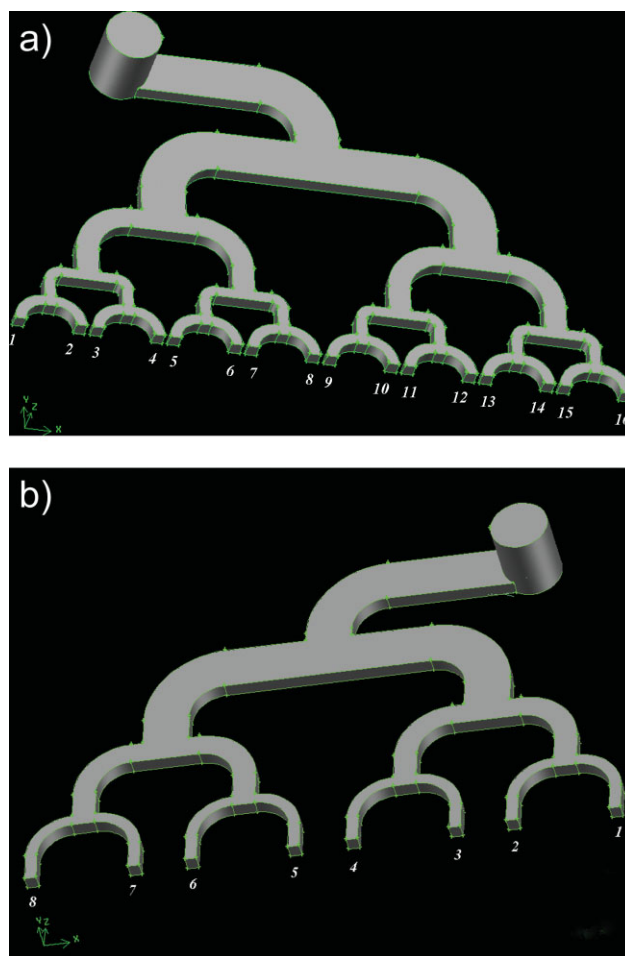


**Figure 3. Schematic overview of the computational domains of constructal distributors in CFD simulations: (a) gas side, the outlet ports are labeled from 1 to 16; (b) liquid side, the outlet ports are labeled from 1 to 8.**

[Color figure can be viewed in the online issue, which is available at [www.interscience.wiley.com](http://www.interscience.wiley.com).]

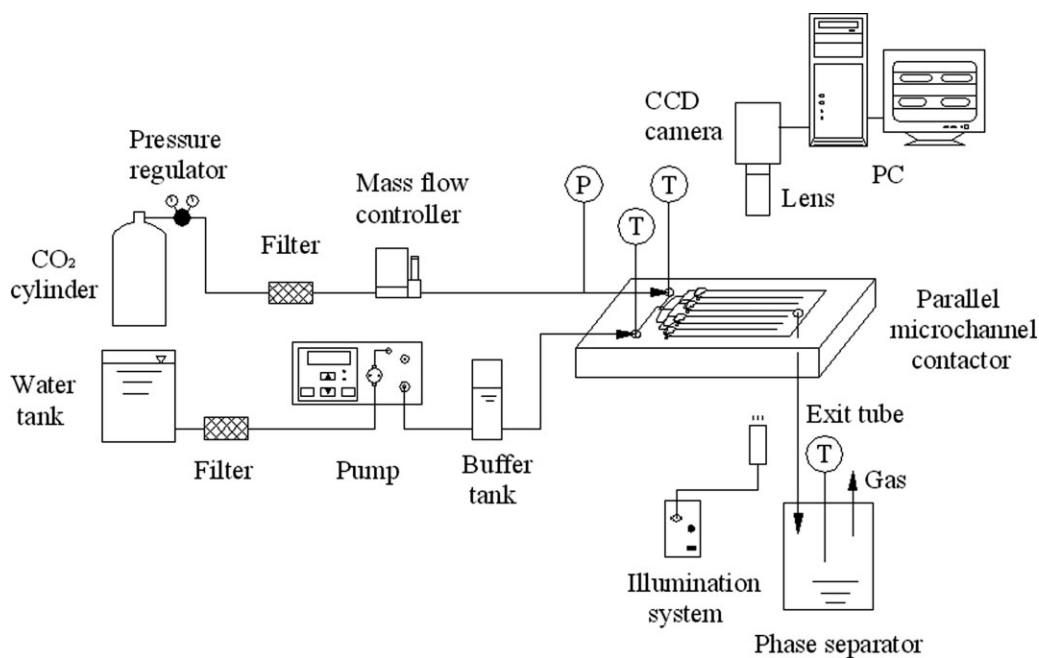


**Figure 4. Schematic of the experimental apparatus for gas-liquid flow distribution and mass transfer study in the parallel microchannel contactor.**

conducted under the inlet water mass flow rate ranging from 0.574 to 5.78 kg/h, corresponding to a Reynolds number within the range of 84–850 in the inlet channel, thus the solver used was always laminar. For the gas side distributor, the inlet CO<sub>2</sub> mass flow rate under simulations varies from 0.027 to 0.39 kg/h, corresponding to a Reynolds number within the range of 241–3526 in the inlet channel. Therefore, the laminar flow solver was used at low flow rates (<0.27 kg/h) whereas the turbulent solver was used at high ones.

#### ***Experimental characterization of two-phase flow distribution and mass transfer in parallel microchannels***

Two-phase flow distribution characteristics during CO<sub>2</sub>-water flow in the present parallel microchannel contactor have been investigated at varying flow conditions, where the overall mass transfer efficiency was also measured simultaneously under most circumstances. A description of the test facilities is schematically shown in Figure 4. Pure CO<sub>2</sub> was supplied from a gas cylinder, the pressure of which was adjusted by a pressure regulator. The possible particulate contamination in CO<sub>2</sub> stream was removed by a filter. A constant flow rate of CO<sub>2</sub> was generated by a mass flow controller with a flow range of 0–10 SLM (here SLM designates standard liters per minute) and then CO<sub>2</sub> entered into the contactor that was placed horizontally through one inlet port. The pressure in the gas feeding line at a certain distance from the inlet port was measured by a pressure transducer with a range of 0–100 kPa. The liquid phase used was boiled deionized water that was stored in a clean tank. Via one or several piston pumps connected in parallel, water at the desired flow rate (up to 100 cm<sup>3</sup>/min) was drawn from the tank and was finally fed into the contactor through the other inlet port. A filter was also used in the liquid line to avoid contaminations. A buffer tank right next to the pump served

to minimize the flow rate pulsation and the accurate mass flow rate of water was actually determined by weighing method. After the introduction of gas and liquid into the contactor, two-phase contacting was realized in 16 parallel microchannels due to the presence of construal distributors, thus leading to the absorption of CO<sub>2</sub> into water. Two-phase mixture from each microchannel then reached the collecting chamber, flowed out of the contactor through the outlet port, and was finally discharged downward into a phase separator by means of a short 4 mm inner diameter polyethylene pipe. For mass transfer measurement consideration, the phase separator was sealed tightly and the unabsorbed CO<sub>2</sub> was guided to flow out of the separator via a sufficient long capillary to prevent air from diffusing into the separator. Three thermocouples (K-type) were placed in the two inlet ports and the phase separator, respectively, to measure the corresponding temperatures. When gas-liquid flow experiments were stopped, CO<sub>2</sub> concentration in water collected in the phase separator was analyzed by using the standard titration method, i.e., by adding the liquid sample from the separator into an excess of NaOH solution and titrating against HCl solution using phenolphthalein and methyl orange as the indicators for the first and second end-points, respectively. All experiments were performed at room temperature and atmospheric pressure (about 20°C, 0.1 MPa).

Under each operational condition, two-phase flow images in the middle section of 16 microchannels (3 cm from the entrance) were recorded with the aid of a high-speed photography system. The key component of this system is a high-performance CCD camera (Uniq UC 610) which can capture images with full frame resolution of 659 × 494 pixel at a frame rate of 110 fps and a shutter speed as high as 110,000 1/s. The magnification of the interested microchannel section was realized by the use of a macro lens coupled with extension tubes. For the best visualization, the camera was placed above the

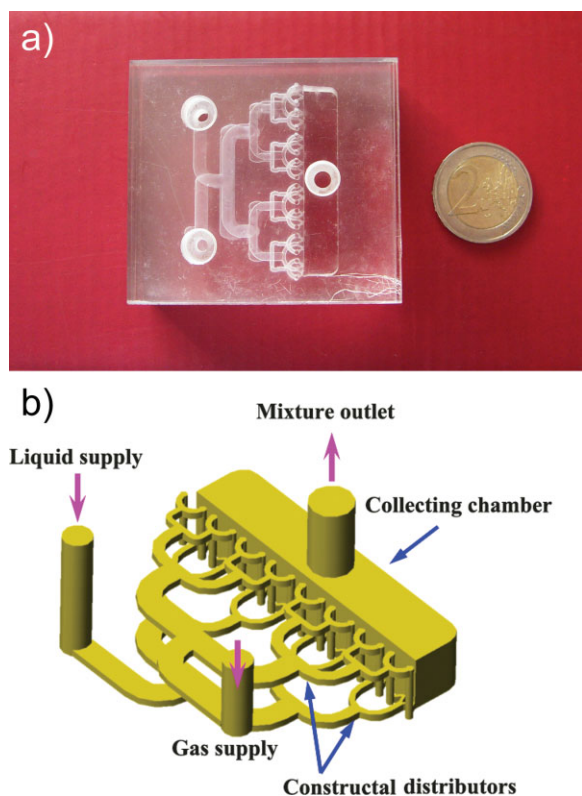


**Figure 5. Reference contactor for estimating mass transfer end effects: (a) photo of the contactor and a coin of 2 euro; (b) internal channel structure.**

[Color figure can be viewed in the online issue, which is available at [www.interscience.wiley.com](http://www.interscience.wiley.com).]

contactor while a strong background illumination was provided by a fiber optic cold light source positioned beneath the contactor. The captured frames were first stored in the memory of a personal computer and were then transferred into the hard disk via a data acquisition system for later analysis.

In the present contactor, a direct measurement of  $\text{CO}_2$  concentration in water flowing in parallel microchannels is impossible. Hence an indirect measurement approach was further used here to derive the interested mass transfer data in these microchannels. In detail, the equivalent mass transfer contribution in the outlet zone of the present contactor during the experiments described earlier (including the collecting chamber, the exit pipe, and the phase separator) was estimated by conducting another set of reference experiments under the same inlet mass flow rates of gas and liquid using an additional contactor shown in Figure 5 (termed as “reference contactor” hereafter). The other experimental setup remained identical to that depicted in Figure 4. From Figure 5 it can be seen that the reference contactor differs in its design from the parallel microchannel contactor in the aspect that the microchannel array for two-phase contacting no longer exists and thus two constructal distributors are directly fed with the collecting chamber. The whole contactor assembly was formed by gluing three acrylic plates together using transparent double sided tapes. The top cover plate comprises two inlet ports for gas and liquid and one outlet port

for two-phase mixture. The middle channel plate consists of two constructal distributors on its both surfaces and the collecting chamber which were machined using a precision micro milling machine. The bottom cover plate is smooth without any channel structure.

#### *Evaluation of the average superficial velocity*

For  $\text{CO}_2$ -water flow in parallel microchannels, the average superficial gas and liquid velocities,  $j_G$  and  $j_L$ , are defined as

$$j_G = \frac{m_{G, \text{tot}}}{\rho_G nHW} \quad (1)$$

$$j_L = \frac{m_{L, \text{tot}}}{\rho_L nHW} \quad (2)$$

where  $n = 16$  for the current parallel microchannel contactor. In view of the fact that there was a somewhat significant pressure variation in the contactor, the gas density in Eq. 1 was evaluated based on the average pressure between the entrance and the outlet of parallel microchannels which was estimated using the same method as that proposed for single microchannel contactors in our previous work.<sup>22</sup> In brief, the static pressures at the entrance and the outlet of parallel microchannels,  $P_0$  and  $P_1$ , were calculated as

$$P_0 = P_{\text{in, PMC}} - \Delta P_{\text{single phase}} \quad (3)$$

$$P_1 = P_0 - \Delta P_T \quad (4)$$

where

$$\Delta P_T = P_{\text{in, PMC}} - P_{\text{in, RC}} \quad (5)$$

In the above equations,  $P_{\text{in, PMC}}$  and  $P_{\text{in, RC}}$  denote the measured inlet pressures in the gas feeding line during two sets of  $\text{CO}_2$ -water experiments in the parallel microchannel contactor and the reference contactor, respectively,  $\Delta P_T$  denotes two-phase total pressure drop in parallel microchannels, and  $\Delta P_{\text{single phase}}$  is the pressure drop caused by gas flow from the pressure measuring point to the entrance of parallel microchannels (including the frictional pressure drops through the feeding line and the gas side constructal distributor as well as the local pressure losses therein). The approximate value of  $\Delta P_{\text{single phase}}$  could be measured from the additional  $\text{CO}_2$  single-phase flow experiments conducted in the reference contactor (with its outlet port directly exposed to air) using the test facilities shown in Figure 4. In other words, the pressure losses associated with  $\text{CO}_2$  flow in the collecting chamber and its discharge into air through the outlet port in such experiments were thought to be unimportant as compared with  $\Delta P_{\text{single phase}}$ . Thus, the measured inlet pressure in the gas feeding line could be regarded as a reasonable estimation of  $\Delta P_{\text{single phase}}$ .

## **Results and Discussion**

### *Single-phase flow characteristics in constructal distributors*

CFD simulations have been performed in two constructal distributors used in the present contactor design to investigate their flow distribution performance under different inlet flow rates. To simplify calculation, these distributors were

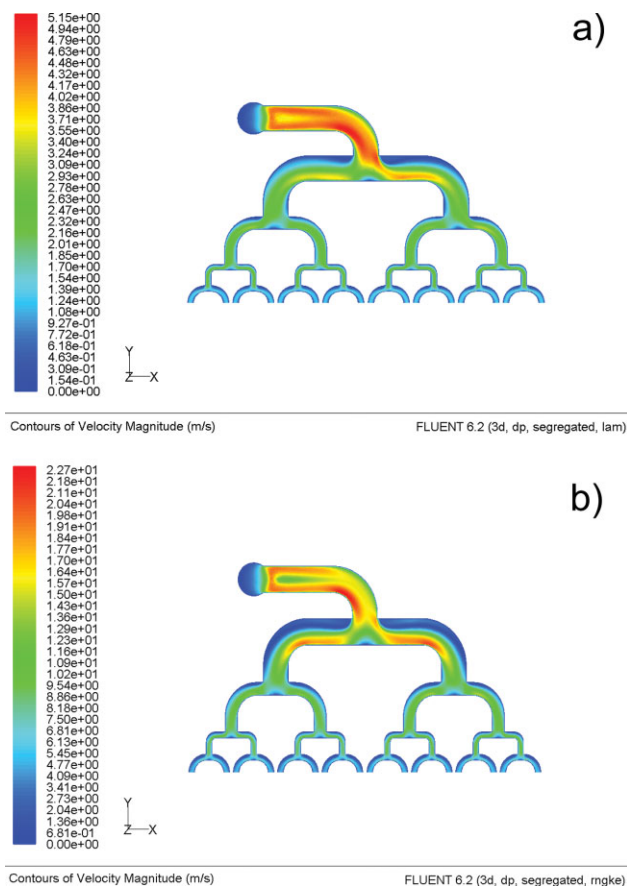


**Figure 6. Contour of velocity magnitude at the central plane inside the gas side distributor: (a)  $m_{G, \text{tot}} = 0.071$  kg/h, corresponding to a mean velocity of 3.37 m/s and a Reynolds number of 650 in the inlet channel; (b)  $m_{G, \text{tot}} = 0.33$  kg/h, corresponding to a mean velocity of 15.6 m/s and a Reynolds number of 3000 in the inlet channel.**

[Color figure can be viewed in the online issue, which is available at [www.interscience.wiley.com](http://www.interscience.wiley.com).]

not coupled with the subsequent microchannel array and the computational domain in the distributor geometry was restricted within several representative generations (Figure 3).

For the gas side distributor, both laminar and turbulent flow cases have been considered. Figure 6a presents the velocity magnitude obtained at the central plane inside this distributor (half the channel depth) under an inlet  $\text{CO}_2$  flow rate of 0.071 kg/h which corresponds to a mean velocity of 3.37 m/s and a Reynolds number of 650 in the inlet channel. It is seen that the velocity profile can be considered as axially symmetric right after the gas enters the inlet channel via the inlet port, although it further develops downstream. However, this symmetry is lost when the gas passes the first elbow after the inlet, which subsequently yields an uneven distribution of the inlet flow between the resulting two channels at the first generation. That is, more fluids are directed into the channel situated at the opposing side of the inlet channel. Moreover, in both channels resulted at this generation, fluids with high velocities are generally positioned next to one side wall whereas a somewhat large stagnant fluid

region presents adjacent to the other side wall. It is also observed that at the first generation, the gas has to pass another elbow and then travels a very short distance before it reaches the inlet of the next generation. Thus, the velocity profile cannot recover its symmetry completely. Typically, a fully-developed Poiseuille velocity field is not established. Consequently, the flow partition at the second generation is also unequal. This trend continues till the last generation where it is expected that the gas flow rates coming out of the resulting 16 channels will be different from each other. When the  $\text{CO}_2$  inlet flow rate further increases, the flow finally becomes turbulent in the inlet channel. In the latter case, the inertial effect is obvious and thus the velocity profile at each generation tends to be more asymmetric (Figure 6b). As a result, a comparatively large flow maldistribution is anticipated.

For the liquid side distributor, the simulations have been carried out under the inlet water flow rate lower than about 6 kg/h, where the flow remains laminar throughout the distributor. Figure 7 shows a typical map of the velocity magnitude obtained at the central plane inside this distributor. The flow characteristics herein generally follow the same trend as in the gas side distributor. In brief, an axially symmetrical velocity profile is usually not ensured at the inlet of each generation primarily due to the presence of the elbows, implying that liquid flow equipartition is also not achieved in the eight outlet ports at the third generation.

To quantify the degree of flow nonuniformity in each distributor, the relative deviation of the actual flow rate in each outlet port from the average flow rate in uniform distribution case is defined here as

$$E_{G,i} = \frac{m_{G,i} - \frac{1}{16} \sum_{i=1}^{16} m_{G,i}}{\frac{1}{16} \sum_{i=1}^{16} m_{G,i}} \quad (6)$$

$$E_{L,i} = \frac{m_{L,i} - \frac{1}{8} \sum_{i=1}^8 m_{L,i}}{\frac{1}{8} \sum_{i=1}^8 m_{L,i}} \quad (7)$$

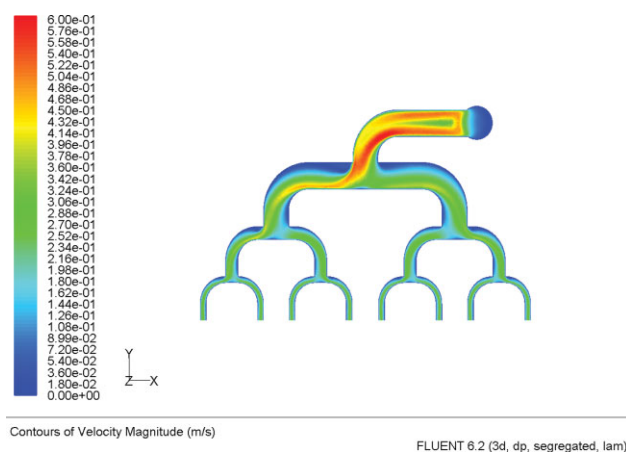


**Figure 7. Contour of velocity magnitude at the central plane inside the liquid side distributor:  $m_{L, \text{tot}} = 4.02$  kg/h, corresponding to a mean velocity of 0.35 m/s and a Reynolds number of 600 in the inlet channel.**

[Color figure can be viewed in the online issue, which is available at [www.interscience.wiley.com](http://www.interscience.wiley.com).]

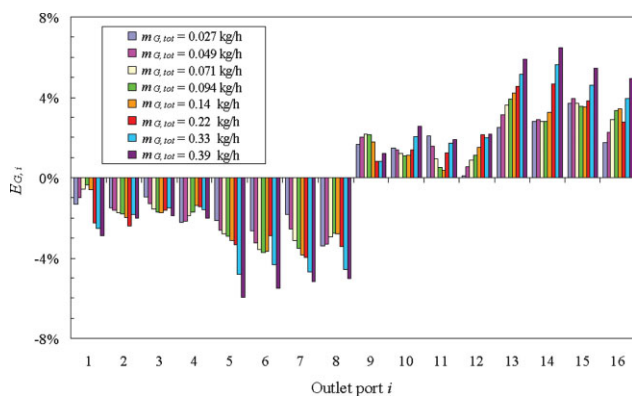


**Figure 8. Variation of  $E_{G,i}$  with the inlet  $\text{CO}_2$  flow rate in the gas side constructal distributor.**

[Color figure can be viewed in the online issue, which is available at [www.interscience.wiley.com](http://www.interscience.wiley.com).]

Figures 8 and 9 depict the variations of  $E_{G,i}$  and  $E_{L,i}$  with the inlet flow rate for the gas side and liquid side distributors, respectively. In two distributors, it is both seen that the flow rates in the outlet ports located at the opposite side of the inlet channel (i.e., ports 9–16 for gas and ports 5–8 for liquid, also see Figure 3) normally exceed above the average value while those in the outlet ports located at the same side of the inlet channel are generally lower than the average value. As explained in the analysis above, this strong flow unbalance is mainly due to the first elbow just after the inlet. In other words, at the first generation, the channel located at the opposite side of the inlet channel receives more fluids. Thus, the sum of the flow rates from the outlet ports 9–16 for gas or 5–8 for liquid is somewhat higher than half the total flow rate fed into the distributor. Furthermore, it is observed that the flow rates in these outlet ports also differ from each other, indicating that the elbows present at the succeeding generations further contribute to uneven flow distribution. During the flow rate range investigated, flow uniformity in each distributor tends to become worse as the inlet flow rate increases. Amongst all the outlet ports, the maximum deviation of the actual flow rate from the average one was found to be about 6.5% and 5.1% for the gas side and liquid side distributors, respectively. Thus, our CFD simulations suggest that a perfect flow equipartition actually cannot be realized in each distributor. Nevertheless, since the observed deviation is small, it is still reasonable to assume a nearly uniform flow distribution in the present two distributors.

### Two-phase flow distribution in parallel microchannels

The above simulations reveal that the present two constructal distributors perform well when used independently, that is, each distributor can realize the almost even distribution of an input flow onto a surface comprising 16 outlet ports. To further check whether these distributors can be integrated together to ensure a nearly perfect two-phase flow equipartition among parallel microchannels as well, two-phase flow distribution in the parallel microchannel contactor has been investigated experimentally.  $\text{CO}_2$ -water flow pattern has been visualized in 16 microchannels of this contactor under almost the same inlet flow rate range as used in CFD simulations, ranging from 0.027 to 0.41 kg/h for the gas and

from 1.16 to 5.82 kg/h for the liquid. According to Eqs. 1 and 2, the average superficial gas and liquid velocities in these microchannels were calculated to be in the range of 0.50–7.69 and 0.04–0.20 m/s, respectively.

If two-phase flow distribution was always uniform among all microchannels, only one specific flow pattern would be observed under each operational condition. This ideal flow pattern can be predicted according to our previously developed flow pattern map for one single microchannel with  $d_h = 667 \mu\text{m}$  which has exactly the same dimensions (i.e., cross-sectional sizes and length) as each of parallel microchannels in the present contactor.<sup>22</sup> Under the average superficial velocities investigated in the present experiments, the ideal flow pattern involved was found to be slug flow or slug-annular flow. In addition, two subregimes can be further identified in slug flow as Taylor flow and unstable slug flow (see Ref. 22 for more information).

Figure 10 gives some typical flow pattern pictures in 16 microchannels at different  $j_G$  and  $j_L$ . For ease of comparison with each other, these microchannels were labeled from 1 to 16. From this figure, the following observations can be made:

- (1) When  $j_G$  was very low, a significant two-phase flow maldistribution across parallel microchannels was noticed. For example, it can be seen from Figure 10a that at  $j_G = 0.50$  m/s, liquid alone flow existed in seven microchannels (channels 1–3, 7, 9, 11, and 13) whereas Taylor flows with different lengths of bubbles were found in some other 6 channels (channels 4–6, 8, and 14–15). Moreover, unstable slug flow dominated in channel 12 and the last two channels (channels 10 and 16) were operated under slug-annular flow. At  $j_G$  and  $j_L$  relevant to this figure, the ideal flow pattern in the case of uniform flow distribution should be Taylor flow according to the flow pattern map previously observed for one single microchannel.<sup>22</sup> Thus, the coexistence of four different flow patterns, especially the presence of liquid alone flow in many channels, indicates that a large flow maldistribution did occur under such circumstances.
- (2) When  $j_G$  was gradually increased at a fixed  $j_L$ , an improvement in two-phase flow uniformity was expected. The most important proof lies in the fact that the number of channels occupied by liquid alone flow (denoted as  $n_{LA}$ )

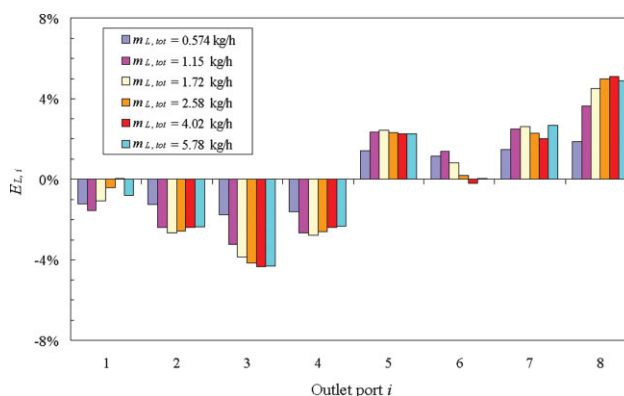


**Figure 9. Variation of  $E_{L,i}$  with the inlet water flow rate in the liquid side constructal distributor.**

[Color figure can be viewed in the online issue, which is available at [www.interscience.wiley.com](http://www.interscience.wiley.com).]



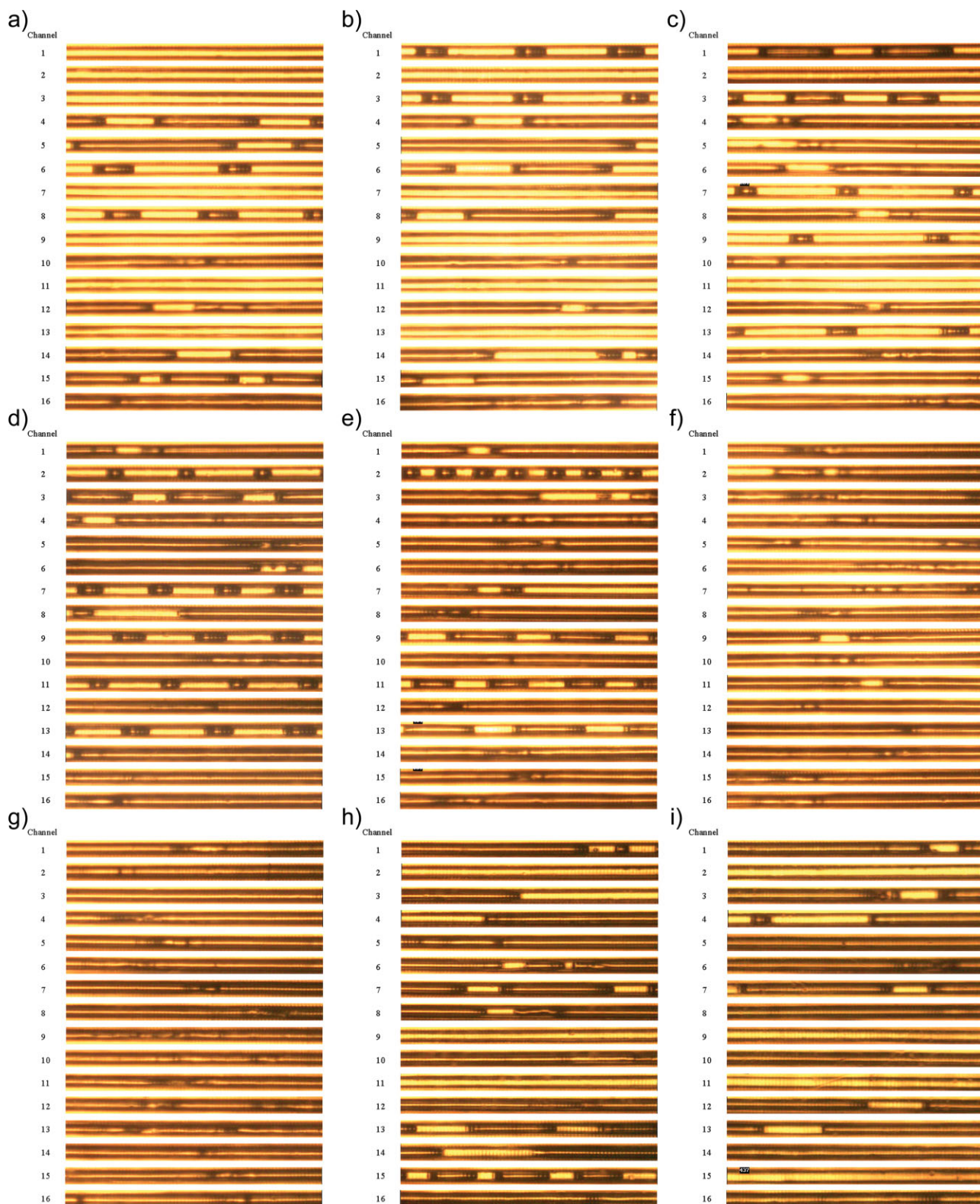


**Figure 10.** Photos of CO<sub>2</sub>-water flow pattern in 16 parallel microchannels (flow direction is from left to right and the observation point is at a distance of 3 cm from the entrance of each microchannel): (a)  $j_G = 0.50$  m/s,  $j_L = 0.14$  m/s; (b)  $j_G = 0.93$  m/s,  $j_L = 0.14$  m/s; (c)  $j_G = 1.35$  m/s,  $j_L = 0.14$  m/s; (d)  $j_G = 1.76$  m/s,  $j_L = 0.14$  m/s; (e)  $j_G = 2.60$  m/s,  $j_L = 0.14$  m/s; (f)  $j_G = 4.23$  m/s,  $j_L = 0.14$  m/s; (g)  $j_G = 6.25$  m/s,  $j_L = 0.14$  m/s; (h)  $j_G = 1.78$  m/s,  $j_L = 0.09$  m/s; (i)  $j_G = 1.78$  m/s,  $j_L = 0.04$  m/s.

[Color figure can be viewed in the online issue, which is available at [www.interscience.wiley.com](http://www.interscience.wiley.com).]

decreases with increasing  $j_G$ . For example, it is seen from Figures 10a–g that  $j_G$  varied from 0.50 to 6.25 m/s while  $j_L$  was kept constant at 0.14 m/s. As compared with Figure 10a ( $n_{LA} = 7$ ), it is obvious in Figure 10b that flow patterns in channels 1 and 3 have changed from liquid alone flow to Taylor flow when  $j_G$  was raised from 0.50 to 0.93 m/s, leaving the remaining five channels still free of gas (channels 2, 7, 9, 11, and 13). At slightly higher  $j_G$  of 1.35 m/s (Figure 10c), only two channels (channels 2 and 11) did not contain gas. Finally, at much higher  $j_G$  of 1.76 m/s (Figure 10d), both gas and liquid coexisted in all channels although flow patterns still differed from channel to channel. Since a radical shift of flow pattern from liquid alone flow to Taylor flow is a result of a more even distribution of gas flow inside the relevant microchannels, the observed decrease of  $n_{LA}$  upon increasing  $j_G$  at a given  $j_L$  clearly suggests that the degree of two-phase flow maldistribution was reduced as well. Another possible proof may be seen from the fact that the number of channels occupied by the ideal flow pattern in uniform distribution case (denoted as  $n_{ideal}$ ) generally increases with an augmentation in  $j_G$ . This trend is easier to recognize when both gas and liquid are present in all channels (see Figures 10e–g). During the operational conditions relevant to the three figures, the ideal flow pattern should be slug-annular flow. In Figure 10e where  $j_G$  was kept at 2.60 m/s, two-phase flow pattern in nine channels was found to be slug-annular flow (channels 4–6, 8, 10, 12, and 14–16). At the elevated  $j_G$  of 4.23 m/s (Figure 10f), 13 channels were now occupied by slug-annular flow (channels 1, 3–8, 10, and 12–16). When  $j_G$  was further raised to 6.25 m/s (Figure 10g), flow patterns in all microchannels proved to be slug-annular flow, implying that a nearly uniform distribution seemed to occur at such high  $j_G$ .

(3) When  $j_L$  was gradually increased at a fixed  $j_G$ , an improvement in two-phase flow distribution was also observed. This finding can be seen from a comparison among the images shown in Figures 10d, h, and i, where  $j_G$  was fixed at about 1.80 m/s and  $j_L$  ranged from 0.04 to 0.14 m/s. At the lowest  $j_L$  investigated (Figure 10i), liquid alone flow was seen in four channels (channels 2, 9, 11, and 15). As  $j_L$  was raised to 0.09 m/s (Figure 10h), Taylor flow began to occupy channel 15 and the other three channels (channels 2, 9, and 11) still contained liquid only. Then a further increase of  $j_L$  to 0.14 m/s (Figure 10d) led to the coexistence of two phases in all microchannels. As we have suggested earlier, a higher value of  $n_{LA}$  corresponds to a poorer two-phase flow distribution. Thus, it seems that two-phase flow distribution in the current contactor was also improved when further increasing  $j_L$  at a given  $j_G$ .

(4) The extent of two-phase flow uniformity depends crucially on the flow distribution status of each phase among all microchannels. The ideal case is that both gas and liquid are evenly distributed into each microchannel, which is difficult to realize in practical operations. In the current parallel microchannel contactor, the presence of liquid alone flow instead of gas alone flow in some microchannels at comparatively low  $j_G$  implies that flow maldistribution in the gas side was more serious (also see Figure 10a). A further investigation on the structure design used in this contactor may help explain this behavior, which will be discussed elsewhere in this article.

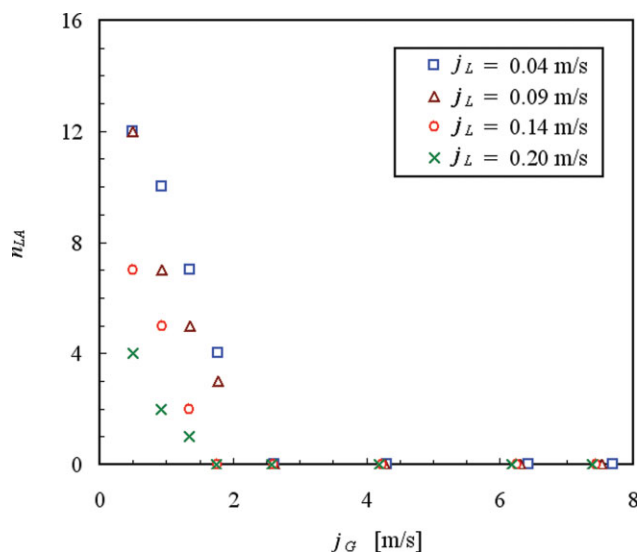


**Figure 11. Measured  $n_{LA}$  as a function of the average superficial gas and liquid velocities for CO<sub>2</sub>-water flow in 16 parallel microchannels.**

[Color figure can be viewed in the online issue, which is available at [www.interscience.wiley.com](http://www.interscience.wiley.com).]

These observations make it clear that the photographic method provides a useful tool for the qualitative characterization of two-phase flow distribution among parallel microchannels of the present contactor. The influence of operational conditions on two-phase flow uniformity can be inferred from the captured flow pattern photos by examining the values of two important variables, namely,  $n_{LA}$  and  $n_{ideal}$ . When liquid alone flow is present in some microchannels, a decrease in the value of  $n_{LA}$  directly means an improvement in flow uniformity. When both gas and liquid coexist in each microchannel, a good flow distribution generally corresponds to a high value of  $n_{ideal}$ . Figures 11 and 12 further describe the variations of  $n_{LA}$  and  $n_{ideal}$  as a function of the average superficial velocities under the present experimental conditions, respectively. It becomes apparent from Figure 11 that  $n_{LA}$  is large at small  $j_G$  and decreases gradually with increasing  $j_G$  or  $j_L$ , implying that two-phase flow maldistribution is alleviated at comparatively high  $j_G$  or  $j_L$ . This conclusion is further corroborated in Figure 12 where it is seen that  $n_{ideal}$  generally increases with increasing  $j_G$  and eventually the ideal flow pattern occupies all microchannels (i.e.,  $n_{ideal} = 16$ ) at very high  $j_G$  for each  $j_L$  investigated. However, it is also noticed that the variation of  $n_{ideal}$  is somewhat irregular especially with respect to  $j_L$  at a fixed  $j_G$ . This irregularity is unavoidable because the difference among inner details in each flow pattern (e.g., length of bubbles or liquid slugs in Taylor flow, widths of liquid film or gas core in slug-annular flow) is not considered during the calculation of  $n_{ideal}$ . Thus, the value of  $n_{ideal}$  sometimes cannot reflect a slight improvement in two-phase flow distribution. In such case, a more reasonable characterization of flow uniformity should be based on a specific knowledge of the precise amounts of gas and liquid fed into each microchannel, which is usually difficult to measure especially when a lot of microchannels are involved.

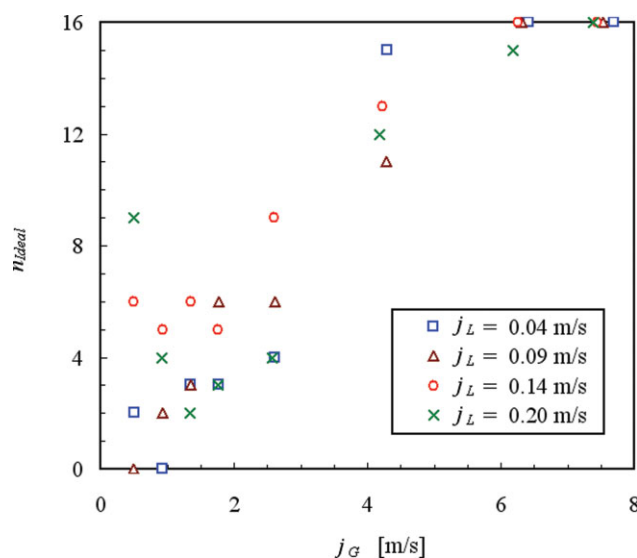


**Figure 12. Measured  $n_{ideal}$  as a function of the average superficial gas and liquid velocities for CO<sub>2</sub>-water flow in 16 parallel microchannels.**

[Color figure can be viewed in the online issue, which is available at [www.interscience.wiley.com](http://www.interscience.wiley.com).]

Recall that in our CFD simulations conducted above, generally a good flow distribution can be assumed for each structural distributor under the present flow rate ranges. Then, one may consider that the integration of these distributors into the present contactor should ensure a nearly uniform distribution of gas and liquid flows into the subsequent parallel microchannels as well. However, our flow visualization experiments have demonstrated that such sort of uniform two-phase flow seemed to occur only at very high  $j_G$  for a fixed  $j_L$  (Figures 10g and 12). At very low  $j_G$  or  $j_L$ , a large two-phase flow maldistribution was observed, as was characterized by the presence of liquid alone flow in many channels (Figures 10a and 11). The total blockage of gas flow in these channels implies that at least the gas side distributor could not function well under these circumstances, which is unexpected according to the simulation results. In fact, the flow inside each distributor in our CFD simulations was simply treated as a steady process with two-phase flow in parallel microchannels being not taken into account. Therefore, a detailed investigation of two-phase hydrodynamics in parallel microchannels and its interaction with fluid flow in the two distributors is necessary to elucidate the poor flow distribution performance under such circumstances.

From Figure 11 it is further seen that liquid alone flow disappeared from all microchannels at  $j_G$  of about 2 m/s, which approximately corresponds to the transition line from slug flow to slug-annular flow observed in one single microchannel.<sup>22</sup> In other words, a significant two-phase flow maldistribution occurred when the ideal flow pattern in parallel microchannels turned to be slug flow. As demonstrated in our previous work,<sup>22</sup> slug flow can be further divided into Taylor flow and unstable slug flow. The two subregimes are intrinsically transient due to the alternative movement of the liquid slug and the gas bubble down the microchannel. Consequently, slug flow is usually accompanied by significant

pressure fluctuations. Salman et al.<sup>34</sup> have found that a pressure fluctuation would be generated when a Taylor bubble burst at the microchannel outlet, which was mostly due to the pressure difference between the inside and the outside of the bubble caused by surface tension. The magnitude of this pressure fluctuation can be estimated from the following Laplace equation when the outlet of the microchannel is directly open to atmosphere,

$$\Delta P_{fluc} \approx \frac{4\sigma}{d_h} \quad (8)$$

Because of the small diameter of the microchannel, this type of pressure fluctuation is usually not negligible especially when two-phase pressure drop across the microchannel is not sufficiently large. Under this circumstance, this type of pressure fluctuation will not only affect the movement of other Taylor bubbles in the microchannel but also the bubble formation process at the microchannel entrance.<sup>34</sup> van Steijn et al.<sup>35</sup> have observed another type of pressure fluctuation associated with the bubble formation at the microchannel entrance. They claimed that such pressure fluctuation was also very important for cases with long bubbles and short liquid slugs. Moreover, the external pressure fluctuation will be present if the flow rate pulsation inside the gas or liquid feeding system (including pumps, feeding lines, etc.) is not eliminated.<sup>36,37</sup> A large external pressure fluctuation may even cause a periodical change among different flow patterns inside the microchannel. When there is only one microchannel involved, the above-mentioned different types of pressure fluctuation can lead to two-phase flow instability. Nevertheless, the dominant flow pattern inside the microchannel still remains to be slug flow because gas and liquid have no other path to flow out of the system. However, if several or more microchannels are operated in parallel, pressure fluctuations in different microchannels will interact in a complicated way. Because bubbles in these microchannels do not form and leave simultaneously, dynamic pressure fluctuation will occur.<sup>19</sup> Notably, de Mas et al.<sup>11</sup> have found that such dynamic pressure fluctuation would lead to unequal flow distribution between two microchannels when the pressure drops inside the gas and liquid distributors were negligibly small and eventually different flow patterns coexisted in these microchannels. Therefore, they suggested that the inlet channels of gas and liquid in the corresponding distributors should be designed to present pressure drops significantly higher than that across the microchannels. Under this condition, the undesired external pressure fluctuation resulting from the feeding system is minimized and the pressure fluctuation associated with slug flow itself also has little impact on the flow inside the distributors.<sup>37</sup> As a result, a uniform slug flow may be realized in each microchannel. This assumption has been further verified by their recent experiments.<sup>26</sup>

In the present parallel microchannel contactor, a large two-phase flow maldistribution was observed when it was designed to be operated under slug flow. Based on the above analysis, it can be concluded that in this case fluid flow inside each structural distributor has been greatly affected by dynamic pressure fluctuation accompanying slug flow in parallel microchannels. It can be seen from Table 1 that the

hydraulic diameters of the resulting channels at the last generation of both distributors are comparable to that of parallel microchannels while the lengths of these distributing channels are much shorter. This means that single-phase pressure drop of gas or liquid substreams through these channels in the respective distributor will be much smaller than two-phase total pressure drop through parallel microchannels. Consequently, due to the lack of high pressure drop channels in the distributors' side as suggested by de Mas et al.,<sup>11</sup> dynamic pressure fluctuation in parallel microchannels would cause flow maldistribution in each distributor, the influence of which was thought to be more pronounced at very low  $j_G$  or  $j_L$ . For example, at the lowest  $j_G$  and  $j_L$  investigated ( $j_G = 0.50$  m/s,  $j_L = 0.04$  m/s), the capillary number ( $Ca = \mu_L U / \sigma$ , where  $U = j_G + j_L$ ) and Weber number ( $We = \rho_L d_h U^2 / \sigma$ ) were calculated to be about 0.007 and 2.7, respectively. According to our previous findings,<sup>22</sup> the bubble formation process at the microchannel entrance under such circumstance could be described by the squeezing mechanism proposed by Garstecki et al.<sup>38</sup> and the effect of inertia on the bubble shape was somewhat significant. That is, the break-up of bubbles at such low  $Ca$  was induced by an inlet liquid pressure fluctuation as the emerging bubble would block almost the entire microchannel cross-section and then a dramatic increase in the liquid pressure upstream was inevitable until the bubble was detached from the gas neck.<sup>39</sup> More importantly, two-phase total pressure drop through the microchannel under this circumstance was not high enough so that it was easy for the pressure fluctuation associated with the burst of the gas bubble at the microchannel outlet to propagate back to the microchannel entrance (according to our previous experiments in one single microchannel,<sup>22</sup> two-phase total pressure drop through the microchannel was found to be around 0.5 kPa at this specified condition;  $\Delta P_{\text{fluc}}$  amounted to be a comparable value of about 0.4 kPa when calculated using Eq. 8 since in the current contactor design a large volume collecting chamber is directly fed with the outlet of each microchannel). As a result, a significant dynamic pressure fluctuation would exist in parallel microchannels and eventually a large flow maldistribution would be incurred in each distributor. In view of the fact that gas is more compressible and that the pressure drop of gas through the corresponding distributor is much smaller than that of liquid under the operational conditions relevant to slug flow, flow distribution in the gas side should be much poorer than that in the liquid side. Thus, it has been seen from our experiments that gas was absent from many microchannels when  $j_G$  or  $j_L$  was very small (Figures 10a and 11). As  $j_G$  or  $j_L$  was gradually increased, two-phase total pressure drop through parallel microchannels became more significant as compared with the induced pressure fluctuation from the outlet. Also the fluid pressure at the microchannel entrance would increase so that the inlet pressure fluctuation associated with the bubble formation might become less important. In such case, flow uniformity inside each distributor was affected by dynamic pressure fluctuation to a somewhat less extent. Consequently, more and more microchannels were found to be occupied by slug flow (Figures 10b, c).

Finally, as  $j_G$  was further increased such that the ideal flow pattern shifted from slug flow to slug-annular flow,

dynamic pressure fluctuation among parallel microchannels was thought to be dampened to a large extent since in the latter flow pattern the gas bubbles have merged into a continuous gas core flowing in the center part of the microchannel.<sup>22</sup> Furthermore, the amplitude of pressure fluctuation in each microchannel was also much smaller than two-phase total pressure drop therein, which was especially the case at very high  $j_G$ . Thus, two-phase flow in parallel microchannels could be essentially treated as steady, implying that the flow inside each constructal distributor could be approximately represented by our CFD simulations. As shown in Figures 8 and 9, the symmetrical tree-like networks present in the two distributors can generally ensure a good gas-liquid distribution. Hence, it has been observed from our experiments that most or all microchannels were occupied by the same slug-annular flow pattern when  $j_G$  was comparatively high (Figures 10f, g), suggesting that two-phase flow uniformity was greatly improved.

Another factor that contributes to the above-mentioned flow maldistribution is the manufacturing tolerance. The method of fabrication used for the present contactor, laser stereolithography, is still in its development stage in terms of shaping microstructures.<sup>40</sup> Thus, it is likely to have imperfections and irregularities in fabrication and a maximum channel-to-channel dimensional difference on the order of 10  $\mu\text{m}$  is not impossible.<sup>27,40</sup> Bearing in mind that an acceptable manufacturing tolerance can even affect single-phase flow distribution in parallel microchannels significantly,<sup>41</sup> we think this factor of second importance in causing the observed two-phase flow maldistribution in the present contactor based on the consideration that the absence of gas flow from many microchannels at small  $j_G$  or  $j_L$  could not be well explained by the impact of this factor alone. In other words, this type of maldistributed flow was mainly attributed to the strong influence of dynamic pressure fluctuation in parallel microchannels due to the lack of large pressure barrier inside each constructal distributor and the possible channel dimensional variations would exacerbate this maldistribution. However, the manufacturing tolerance should be paid enough attention when conceiving the improved design of the current contactor that can afford an ideal two-phase flow equipartition.

### *Mass transfer in parallel microchannels*

To keep the desired mass transfer characteristics during the numbering-up process of microchannel contactors, it is a requisite to have uniform two-phase flow patterns in parallel microchannels. However, a perfect two-phase flow equipartition across a multitude of microchannels is usually not easy to realize especially when the interested flow pattern is slug flow, as revealed in our flow visualization experiments. In that case, a systematic deviation of mass transfer performance from its optimal level is anticipated, which should be interpreted based on the knowledge of two-phase flow distribution status therein.

During CO<sub>2</sub>-water flow in the present parallel microchannel contactor, mass transfer measurements were also performed to derive the average liquid side volumetric mass transfer coefficient  $(k_L a)_{\text{avg}}$  in 16 microchannels. To better explain the obtained data, the impact of two-phase flow

distribution on mass transfer in these microchannels should be made clear. Therefore, a simplified analysis is first given here. The difference in mass transfer performance between nonuniform and uniform flow distribution cases can be evaluated by using the following expression<sup>42</sup>

$$E_r = \frac{(k_L a)_{\text{avg}} - (k_L a)_{\text{uni}}}{(k_L a)_{\text{uni}}} \quad (9)$$

Here  $(k_L a)_{\text{uni}}$  is the optimal liquid side volumetric mass transfer coefficient in parallel microchannels when uniform flow distribution occurs, which should be well predicted by the empirical correlations that we have proposed to describe mass transfer characteristics for CO<sub>2</sub>-water system in one single microchannel (see Ref. 9). In detail, if the ideal flow pattern involved is slug flow, there should be

$$\frac{k_L a d_h^2}{D_L} = 0.084 R e_{\text{GS}}^{0.213} R e_{\text{LS}}^{0.937} S c_L^{0.5} \quad (10)$$

And if the ideal flow pattern is slug-annular flow, there should be

$$\frac{k_L a d_h^2}{D_L} = 0.058 R e_{\text{GS}}^{0.344} R e_{\text{LS}}^{0.912} S c_L^{0.5} \quad (11)$$

When two-phase flow maldistribution occurs, the corresponding  $(k_L a)_{\text{avg}}$  represents an average measurement of CO<sub>2</sub> absorption efficiency in parallel microchannels and can be calculated as

$$(k_L a)_{\text{avg}} = \frac{j_L}{\Delta L} \ln \left( \frac{C^* - C_{\text{in}}}{C^* - C_{\text{mix}}} \right) \quad (12)$$

where  $C_{\text{mix}}$  is the mixed cup CO<sub>2</sub> concentration in water at the outlet of parallel microchannels given by

$$C_{\text{mix}} = \frac{1}{n j_L} \sum_{i=1}^n j_{L,i} C_{\text{ch},i} \quad (13)$$

In this equation,  $j_{L,i}$  and  $C_{\text{ch},i}$  are the actual superficial liquid velocity and the outlet CO<sub>2</sub> concentration in water in microchannel  $i$ , respectively. The value of  $C_{\text{ch},i}$  can be further derived from the equation that defines the actual liquid side volumetric mass transfer coefficient in microchannel  $i$ , that is,

$$(k_L a)_i = \frac{j_{L,i}}{\Delta L} \ln \left( \frac{C^* - C_{\text{in}}}{C^* - C_{\text{ch},i}} \right) \quad (14)$$

Note that when the flow pattern in this microchannel turns to be slug flow or slug-annular flow,  $(k_L a)_i$  can be estimated with Eq. 10 or 11 as well (the actual superficial gas and liquid velocities,  $j_{G,i}$  and  $j_{L,i}$ , should be used to calculate the corresponding superficial Reynolds numbers as required in the two equations). Since other flow patterns (bubbly, churn, annular, liquid alone, and gas alone flows) are likely to exist in microchannels depending on the degree of flow maldistribution, it is further assumed here that Eq. 10 is valid for

bubbly flow case and that Eq. 11 can be used for flow patterns including churn and annular flows. For liquid alone or gas alone flow,  $(k_L a)_i$  should be 0. This can be predicted by either equation.

By combining Eqs. 9–14, it is finally obtained that under the ideal flow pattern of slug flow,  $E_r$  is expressed as

$$E_r = \left[ -\frac{j_L^{0.063}}{0.084 A^{0.15} j_G^{0.213}} \ln \left( \sum_{i=1}^k \left( \frac{j_{L,i} e^{-0.084 A^{0.15} j_G^{0.213} j_{L,i}^{-0.063}}}{n j_L} \right) \right) + \sum_{i=k+1}^n \left( \frac{j_{L,i} e^{-0.058 B^{0.256} j_G^{0.344} j_{L,i}^{-0.088}}}{n j_L} \right) \right] - 1 \quad (15)$$

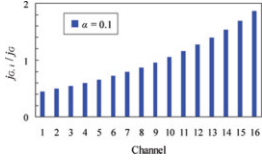
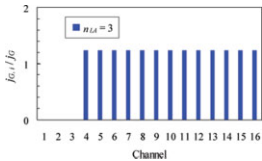
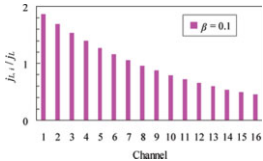
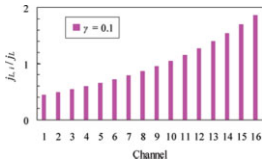
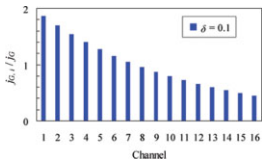
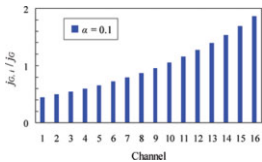
and the following equation exists when the ideal flow pattern shifts to slug-annular flow

$$E_r = \left[ -\frac{j_L^{0.088}}{0.058 B^{0.256} j_G^{0.344}} \ln \left( \sum_{i=1}^k \left( \frac{j_{L,i} e^{-0.084 A^{0.15} j_G^{0.213} j_{L,i}^{-0.063}}}{n j_L} \right) \right) + \sum_{i=k+1}^n \left( \frac{j_{L,i} e^{-0.058 B^{0.256} j_G^{0.344} j_{L,i}^{-0.088}}}{n j_L} \right) \right] - 1 \quad (16)$$

In the above two equations,  $A = \frac{D_L^{6.67} \Delta L^{6.67} S c_L^{3.33}}{d_h^{8.67} v_G^{1.42} v_L^{6.25}}$ ,  $B = \frac{D_L^{3.91} \Delta L^{3.91} S c_L^{1.95}}{d_h^{2.91} v_G^{1.35} v_L^{3.56}}$ , and  $k$  is the number of channels occupied by slug or bubbly flow under maldistributed flow case. Therefore, if the actual superficial gas and liquid velocities in each microchannel are known, the distribution of flow pattern among parallel microchannels is made clear according to the flow pattern map in one single microchannel. Then the relative deviation of the overall mass transfer efficiency in parallel microchannels from its optimal value can be derived using Eq. 15 or 16.

Here a selection of six two-phase flow distribution cases has been considered, as described in Table 2. The first two cases represent the circumstances under which the flow rate of CO<sub>2</sub> increases gradually by a proportion of  $\alpha$  from channels 1 to 16 while the flow rate of water along these channels decreases gradually by a proportion of  $\beta$  (case A) or increases by a proportion of  $\gamma$  (case B). In cases C and D, the gas flow is evenly distributed among certain channels on the right side with the other channels (the number of which is denoted as  $n_{\text{LA}}$ ) being free of gas, and the liquid flow rate distribution is identical to that in cases A and B, respectively. In cases E and F, the liquid flow is now evenly distributed among each channel except the left several ones (the number of which is denoted as  $n_{\text{GA}}$ ) being free of liquid. The gas flow rate from channels 1 to 16, however, decreases gradually by a proportion of  $\delta$  (case E) or increases by a proportion of  $\alpha$  (case F). It is thought that cases A–F can in principle provide a realistic view of gas–liquid distribution status that may occur in the present parallel microchannel contactor during practical operations, which will be further discussed below. Figures 13a–f compare mass transfer performance under the selected two-phase flow distribution cases at  $j_G = 0.50$  m/s and  $j_L = 0.14$  m/s, where the

**Table 2. Two-Phase Flow Distribution Cases Considered in the Analysis [Color table can be viewed in the online issue, which is available at [www.interscience.wiley.com](http://www.interscience.wiley.com).]**

Case	Flow Distribution Configuration			
	Gas Side		Liquid Side	
A		$j_{G,i+1}/j_{G,i} = 1 + \alpha$ $i = 1, 2, \dots, 15$ $\alpha > 0$		$j_{L,i}/j_{L,i+1} = 1 + \beta$ $i = 1, 2, \dots, 15$ $\beta > 0$
B		$j_{G,i+1}/j_{G,i} = 1 + \alpha$ $i = 1, 2, \dots, 15$ $\alpha > 0$		$j_{L,i+1}/j_{L,i} = 1 + \gamma$ $i = 1, 2, \dots, 15$ $\gamma > 0$
C		$j_{G,i} = 0$ $i = 1, 2, \dots, n_{LA},$ $j_{G,i} = j_{G,i+1}$ $i = n_{LA} + 1, n_{LA} + 2, \dots, 15$		$j_{L,i}/j_{L,i+1} = 1 + \beta$ $i = 1, 2, \dots, 15$ $\beta > 0$
D		$j_{G,i} = 0$ $i = 1, 2, \dots, n_{LA};$ $j_{G,i} = j_{G,i+1}$ $i = n_{LA} + 1, n_{LA} + 2, \dots, 15$		$j_{L,i+1}/j_{L,i} = 1 + \gamma$ $i = 1, 2, \dots, 15$ $\gamma > 0$
E		$j_{G,i}/j_{G,i+1} = 1 + \delta$ $i = 1, 2, \dots, 15$ $\delta > 0$		$j_{L,i} = 0$ $i = 1, 2, \dots, n_{GA};$ $j_{L,i} = j_{L,i+1}$ $i = n_{GA} + 1, n_{GA} + 2, \dots, 15$
F		$j_{G,i+1}/j_{G,i} = 1 + \alpha$ $i = 1, 2, \dots, 15$ $\alpha > 0$		$j_{L,i} = 0$ $i = 1, 2, \dots, n_{GA},$ $j_{L,i} = j_{L,i+1}$ $i = n_{GA} + 1, n_{GA} + 2, \dots, 15$

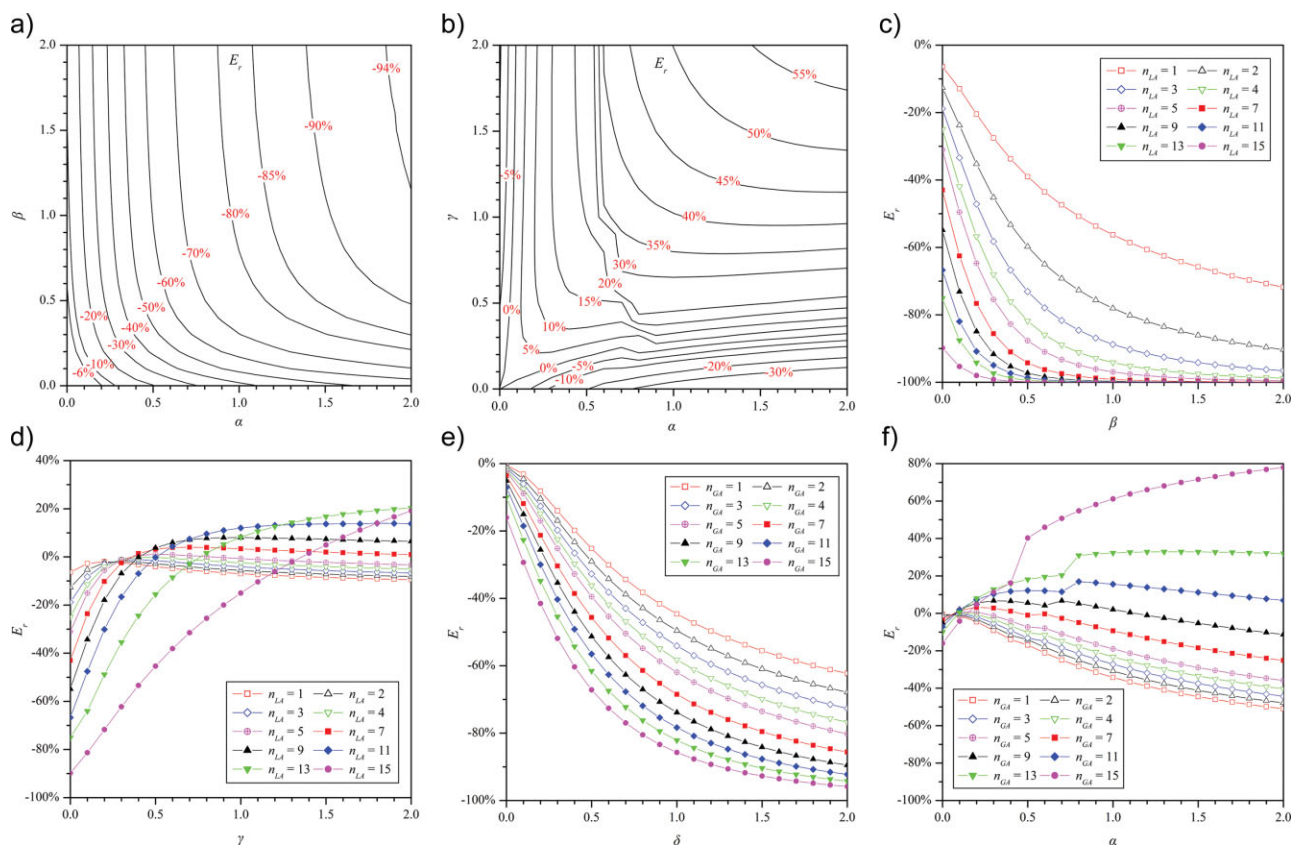


**Figure 13. Mass transfer performance in 16 parallel microchannels under different two-phase flow distribution cases at  $j_G = 0.50$  m/s,  $j_L = 0.14$  m/s,  $20^\circ\text{C}$ , 101 kPa: (a) case A; (b) case B; (c) case C; (d) case D; (e) case E; (f) case F.**

[Color figure can be viewed in the online issue, which is available at [www.interscience.wiley.com](http://www.interscience.wiley.com).]

obtained  $E_r$  is plotted as a function of the given flow distribution parameters (i.e.,  $\alpha$ ,  $\beta$ ,  $\gamma$ ,  $\delta$ ,  $n_{GA}$  and  $n_{LA}$ ) in a two-dimensional contour or scatter graph. The relevant findings that can be made from these figures are:

(1) For cases A, C, and E in which the gas and liquid substreams with relatively high flow rates are located on the opposite sides of 16 channels, respectively,  $E_r$  is always lower than 0. For example, it is shown in Figure 13a that when there is a stepwise increase of 10% in the gas flow rate from channels 1 to 16 and the liquid flow rate decreases by the same percentage accordingly (case A:  $\alpha = 0.1$ ,  $\beta = 0.1$ ),  $E_r$  amounts to be about  $-6\%$ . Moreover, as  $\alpha$  or  $\beta$  is further increased,  $E_r$  becomes much lower. Since an increase in  $\alpha$  or  $\beta$  directly translates into a relatively large flow maldistribution in the gas or liquid side, this finding indicates that a poor two-phase flow distribution will lead to the degradation in the overall mass transfer efficiency, which is in accordance with our common sense. The same degradation can be also found in cases C and E (Figures 13c, e). In the latter two figures it is obvious that the more the number of channels occupied by liquid alone or gas alone flow (i.e.,  $n_{LA}$  or  $n_{GA}$ ), the lower the overall mass transfer efficiency. Notably, when  $n_{LA}$  or  $n_{GA}$  takes the value of 15,  $E_r$  approaches  $-100\%$  at comparatively large  $\beta$  or  $\delta$ . In such cases, the majority of gas and liquid are present in totally different channels without contacting between them, and therefore the

absorption of gas into liquid hardly occurs. During the operation of parallel microchannel contactors, the degradation mentioned above is most likely to be present. In detail, it is usually seen that parallel microchannels are fed with common inlet and outlet (or pressure drops through fluid distributors as well as the outlet zone are negligible as compared to that across parallel microchannels), which justifies an assumption of a constant pressure drop in microchannels. Then if the gas flow rate increases gradually across microchannels due to some certain reasons (e.g., improper distributor design), the liquid flow rate therein will decrease accordingly in order to meet the constant pressure drop constraint, as case A describes. Similarly, if one fluid is absent from some microchannels as observed in our experiments, the flow rate of the other fluid therein should be much higher than the average value, which is approximately what cases C and E represent. As a result, the average liquid side volumetric mass transfer coefficient in parallel microchannels will be lower than that under uniform distribution case (i.e.,  $E_r < 0$ ).

(2) For cases B, D, and F in which the gas and liquid substreams with relatively high flow rates are both located on the same side of 16 channels, there are some occasions where  $E_r$  is larger than 0. For example, Figure 13b indicates that  $E_r$  amounts to be about  $5\%$  when the flow rates of gas and liquid both increase by a proportion of 20% from channels 1 to 16 (case B:  $\alpha = 0.2$ ,  $\gamma = 0.2$ ). Furthermore,  $E_r$

increases with increasing  $\alpha$  and  $\gamma$ . In cases D and F, it is also observed that when the value of  $n_{LA}$  or  $n_{GA}$  is above 7 or 11,  $E_r$  tends to be larger than 0 at much high  $\gamma$  or  $\alpha$  (Figures 13d, f). Under the extreme condition, that is,  $\alpha$  and  $\gamma$  become sufficiently large and both  $n_{GA}$  and  $n_{LA}$  take the value of 15, two-phase flow distribution in cases B, D, and F all comes to an extent that gas and liquid are only present in channel 16 (flow pattern therein is estimated to be churn flow under  $j_G$  and  $j_L$  involved here) and the other channels are left empty. Then from Eq. 15 it is easy to obtain that

$$E_r = \left[ \frac{0.058B^{0.256}n^{0.256}j_G^{0.131}}{0.084A^{0.15}j_L^{0.025}} - 1 \right] = 104.5\% \quad (17)$$

In practical operations, these occasions occur less frequently, which may be anticipated when a severe local fouling or even blockage happens accidentally in some channels. Although the observations here suggest that mass transfer rate in such occasions is higher than that in uniform distribution case, it does not imply that a uniform distribution is unimportant. In fact, the system is operated in an abnormal mode especially when most microchannels are blocked. In other words, a small increase in mass transfer coefficient is realized at a cost of a very large pressure drop penalty since large portions of gas and liquid are introduced into the other clean or unblocked channels. From this point of view, the intensified mass transfer here is obviously of no practical value.

(3) When both gas and liquid are present in all channels, the average liquid side volumetric mass transfer coefficient usually shows little deviation from its ideal value so long as there is not a considerably large variation in the flow rates of gas and liquid among these channels. For example, it can be seen from Figures 13a, b that when the values of  $\alpha$ ,  $\beta$ , and  $\gamma$  are all not larger than 0.1 in cases A and B,  $E_r$  only ranges from about  $-6$  to  $0\%$  and  $0$  to  $2\%$ , respectively. Note that under these conditions, the highest standard deviation between the actual flow rate of each phase in 16 microchannels and the average one amounts to be  $44.5\%$ , which was calculated from

$$S_G = \sqrt{\frac{1}{n-1} \sum_{i=1}^n \left( \frac{j_{G,i}}{j_G} - 1 \right)^2} \quad (18)$$

$$S_L = \sqrt{\frac{1}{n-1} \sum_{i=1}^n \left( \frac{j_{L,i}}{j_L} - 1 \right)^2} \quad (19)$$

Thus it suggests that the overall mass transfer efficiency can be still maintained at an acceptable level if two-phase flow distribution does not show large difference from the uniform distribution case, which can be explained in the following way. The absorption rate of  $\text{CO}_2$  in microchannel  $i$ ,  $N_i$ , can be written as

$$N_i = j_{L,i}HW(C_{ch,i} - C_{in}) \quad (20)$$

From Eq. 14,  $N_i$  can be further expressed as

$$N_i = j_{L,i}HW(C^* - C_{in}) \left( 1 - e^{-(k_L a) \frac{\Delta L}{j_{L,i}}} \right) \quad (21)$$

Then with Eqs. 10 and 11, it is easy to find that  $N_i$  will increase when there is an increase in  $j_{G,i}$  or  $j_{L,i}$ . Therefore, the channels with high gas or liquid flow rate will give more amounts of absorption whereas those channels with low gas or liquid flow rate will give less. Under the circumstance in which the flow rate variation in the gas or liquid side is not very significant, it is expected that the absorption process from the above two aspects will compensate with each other to a large extent. Thus the associated  $E_r$  will vary little around 0.

In brief, the above results of analysis have revealed that for physical absorption of  $\text{CO}_2$  into water in 16 parallel microchannels of the present contactor, the overall mass transfer efficiency is greatly affected by two-phase flow uniformity. Normally a large two-phase flow maldistribution will cause a serious deterioration of mass transfer performance. Nevertheless, the desired mass transfer efficiency can be still kept provided two-phase flow distribution does not deviate much from its uniform level.

Besides the simplified analysis performed earlier, mass transfer characteristics in 16 microchannels of the present contactor have been investigated experimentally by physical absorption of  $\text{CO}_2$  into water as well. Under each operational condition, the absorption experiments were conducted in this contactor and the reference contactor shown in Figure 5, respectively. Similar to our mass transfer analysis for one single microchannel,<sup>9</sup> the average liquid side volumetric mass transfer coefficient in parallel microchannels can be measured from the experiments as

$$(k_L a)_{\text{avg}} = \frac{j_L}{\Delta L} \ln \left( \frac{C^* - C_{\text{out,PMC}}}{C^* - C_{\text{out,RC}}} \right) \quad (22)$$

Figures 14a–c illustrate the variation of the measured  $(k_L a)_{\text{avg}}$  values with  $j_G$  at different  $j_L$  ranging from 0.09 to 0.20 m/s, where it is seen that  $(k_L a)_{\text{avg}}$  generally shows a continuous increase with increasing  $j_G$  at a given  $j_L$ . To examine the extent to which the overall mass transfer efficiency in these microchannels deviates from that in uniform distribution case, the obtained  $(k_L a)_{\text{avg}}$  data are further compared with the predictions of Eq. 10 or 11 in the three figures depending on the type of ideal flow pattern involved (i.e., Eq. 10 for slug flow; Eq. 11 for slug-annular flow). It seems that  $(k_L a)_{\text{avg}}$  is in reasonable agreement with the prediction at somewhat higher  $j_G$  for all three  $j_L$  investigated. However, as  $j_G$  becomes very small (typically  $< 1.0$  m/s),  $(k_L a)_{\text{avg}}$  tends to be much lower than the prediction. These observations can be explained based on our analysis described earlier. In the present parallel microchannel contactor, it has been found that a large flow maldistribution occurred at very low  $j_G$  where the ideal flow pattern was slug flow, as was evidenced by the presence of liquid alone flow in a lot of microchannels (e.g.,  $j_G = 0.50$  m/s, see Figure 10a). According to our analysis, if gas is absent from many microchannels (i.e.,  $n_{LA}$  is comparatively large), normally a much lower  $(k_L a)_{\text{avg}}$  value than the ideal one will be yielded (Figure 13c). In other words, a much poorer two-phase



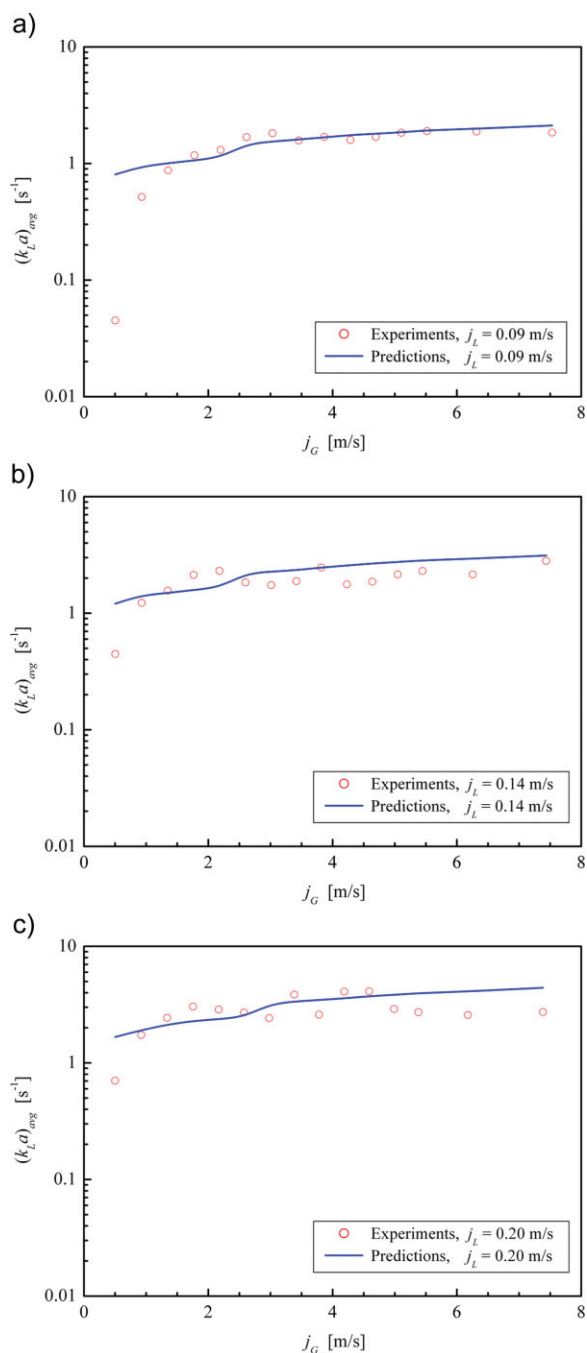


**Figure 14. Measured  $(k_L a)_{\text{avg}}$  value as a function of the average superficial gas velocity and its comparison with the prediction of Eq. 10 or 11 in 16 parallel microchannels: (a)  $j_L = 0.09$  m/s; (b)  $j_L = 0.14$  m/s; (c)  $j_L = 0.20$  m/s.**

[Color figure can be viewed in the online issue, which is available at [www.interscience.wiley.com](http://www.interscience.wiley.com).]

distribution will cause a significant loss in mass transfer efficiency. Thus, it has been seen from Figures 14a–c that  $(k_L a)_{\text{avg}}$  is much lower than the prediction when  $j_G$  is typically small. Upon further increasing  $j_G$ , the number of microchannels

occupied by liquid alone flow decreased gradually. Moreover, at moderate values of  $j_G$ , gas–liquid contacting was realized in each microchannel although several flow patterns coexisted (e.g.,  $j_G = 1.76$  m/s, see Figure 10d). Under this circumstance, two-phase flow maldistribution was mitigated to a large extent, that is, the deviation of the actual gas or liquid flow rate in each microchannel from the average value was thought to be reduced significantly. Our simplified analysis has revealed that mass transfer performance differs little from its optimum level provided there does not exist a considerably large flow rate variation among parallel microchannels. Therefore, it is shown in Figures 14a–c that the experimental  $(k_L a)_{\text{avg}}$  values are generally close to the predictions at moderate values of  $j_G$ . Finally, when  $j_G$  was raised to a very high value, the ideal flow pattern of slug-annular flow was found to be present in the majority or all of parallel microchannels (e.g.,  $j_G = 4.23$  m/s, see Figure 10f), suggesting a nearly uniform two-phase flow distribution. In that case, the measured  $(k_L a)_{\text{avg}}$  values should agree well with the predictions, which is further corroborated by the comparison shown in Figures 14a–c especially for the data concerning the lowest  $j_L$  of 0.09 m/s. For the other two higher  $j_L$  investigated, the experimental data are somewhat scattered possibly due to experimental errors therein. Nevertheless, the predictions are still comparable to the experimental results.

In summary, the results here suggest that the desired mass transfer characteristics in microchannel contactors can be maintained during the numbering-up process so long as two-phase flow distribution in parallel microchannels does not deviate much from its uniform level. In the present work, this acceptable distribution has been realized by the integration of two constructal distributors in front of parallel microchannels. As a result, a significant degradation in the overall mass transfer efficiency has been avoided under a wide range of operational conditions except at very low  $j_G$ . However, it must be pointed out that for the current physical absorption experiments, it is reasonable to use the average liquid side volumetric mass transfer coefficient as a numbering-up criterion because the main objective here is to keep the macroscopic absorption efficiency at its ideal level. When chemical reactions are involved, the complex interplay between mass transfer and chemical kinetics may further complement this objective such that it is also necessary to keep the actual liquid side volumetric mass transfer coefficient in each microchannel close to its optimal value (i.e., an even distribution of  $(k_L a)_i$ ). In the latter case, a two-phase flow distribution as uniform as possible should be guaranteed, which was achieved in the present contactor only at much higher  $j_G$  where the ideal flow pattern was slug-annular flow. To generate a uniform distribution of gas and liquid across microchannels at any ideal flow pattern, the current design should be further improved. As far as slug flow is concerned, one possible means is to incorporate high pressure drop channels in each constructal distributor according to the findings of de Mas et al.<sup>26</sup>

## Conclusions and Future Work

In this article, the feasibility of integrating two constructal distributors into a gas–liquid parallel microchannel contactor has been demonstrated. Each distributor comprises a

dichotomic tree structure with four generations to distribute an inlet gas or liquid stream among the subsequent 16 parallel microchannels with hydraulic diameters of 667  $\mu\text{m}$ . Flow distribution and mass transfer characteristics during  $\text{CO}_2$ -water flow inside this contactor have been investigated both numerically and experimentally.

CFD simulations of single-phase flow through each constructal distributor itself have revealed that the flow partition at each generation of the distributor is actually unequal primarily due to the presence of the elbows. However, a close to uniform distribution of gas or liquid is usually ensured because the flow deviation is small under the operational conditions studied. Unexpectedly, it has been found from our flow visualization experiments that the integration of these two distributors into the present parallel microchannel contactor cannot, in all instances, ensure a nearly uniform two-phase flow distribution. For a given average superficial liquid velocity, a significant flow maldistribution was observed at relatively low average superficial gas velocities where the ideal flow pattern was slug flow. This maldistribution was mainly characterized by the presence of liquid alone flow in many microchannels. Only when the average superficial gas velocity was high enough so that the ideal flow pattern turned to be slug-annular flow, did flow distribution seem to be almost uniform in view of the fact that most or all microchannels were occupied by the same slug-annular flow pattern. A further fluid dynamic analysis has made it clear that the lack of high pressure drop channels in the two constructal distributors was the main cause responsible for the observed large flow maldistribution at relatively low average superficial gas velocities. Under these circumstances, dynamic pressure fluctuation accompanying slug flow in parallel microchannels would greatly disturb an otherwise nearly uniform flow distribution inside each distributor. In contrast, at comparatively high average superficial gas velocities, the impact of dynamic pressure fluctuation was greatly reduced under the ideal flow pattern of slug-annular flow and thus flow distribution in each distributor was hardly affected by two-phase flow in parallel microchannels. In the latter case, the symmetrical tree-like networks inside constructal distributors can guarantee an almost even distribution of gas and liquid in each microchannel, as our CFD simulations correctly reflect.

A simplified analysis has been performed to elucidate the influence of two-phase flow distribution on mass transfer in 16 microchannels of the present contactor. It has been shown that a large two-phase flow maldistribution will lead to a significant deterioration of the overall mass transfer efficiency. However, if two-phase flow distribution does not deviate much from its uniform level, the overall mass transfer efficiency can be still kept at an acceptable level. Based on this analysis, the experimental mass transfer data can be well explained, which confirmed that the desired mass transfer performance previously achieved in one single microchannel could be realized in the present 16 microchannels under a relatively wide operational range due to the integration of two constructal distributors.

Our future work on the improvement of the present contactor design will focus on the optimization of the inner channel structure of both constructal distributors to realize

the ideal two-phase flow equipartition among parallel microchannels. First, the distance traveled by the fluid from the elbow all the way to the inlet of each generation will be arranged long enough to allow the fluid velocity profile to recover its symmetry. Also channels that present much high pressure drops will be incorporated at the last generation to ensure that both distributors function well under slug flow. Then the channel dimensions in the resulted new distributors will be further optimized on the basis of the constructal law under a compromise between the constraints of minimal viscous dissipation and total channel volume.<sup>27</sup> Finally, a new parallel microchannel contactor integrated with the modified distributors will be constructed and its good flow distribution performance will be validated via experimental characterization as well as numerical analysis. Especially, nonintrusive methods for the measurement of fluid flow rate in a number of microchannels are being sought to quantify the degree of two-phase flow uniformity in a more reasonable way.

## Acknowledgments

This work was financially supported by Ministry of Science and Technology of China (Nos. 2009CB219903 and 2007AA030206), National Natural Science Foundation of China (No. 20490208) and the French ANR (Agence Nationale de la Recherche) within the "programme non thématique 2005" (No. NT05-3\_41570).

## Notation

- $A, B$  = constants in Eqs. 15 and 16, s/m
- $C^*$  = physical solubility of  $\text{CO}_2$  in the liquid,  $\text{mol/m}^3$
- $C_{\text{ch},i}$  =  $\text{CO}_2$  concentration in water at the outlet of microchannel  $i$ ,  $\text{mol/m}^3$
- $C_{\text{in}}$  =  $\text{CO}_2$  concentration in water at the entrance of parallel microchannels,  $\text{mol/m}^3$
- $C_{\text{mix}}$  = mixed cup  $\text{CO}_2$  concentration in water at the outlet of parallel microchannels,  $\text{mol/m}^3$
- $C_{\text{out,PMC}}$  =  $\text{CO}_2$  concentration in the phase separator during experiments with the parallel microchannel contactor,  $\text{mol/m}^3$
- $C_{\text{out,RC}}$  =  $\text{CO}_2$  concentration in the phase separator during experiments with the reference contactor,  $\text{mol/m}^3$
- $d_h$  = hydraulic diameter of microchannel, m
- $D_L$  = liquid-phase diffusivity,  $\text{m}^2/\text{s}$
- $E_{G,i}$  = relative flow rate deviation in the outlet port  $i$  locating at the last generation of the gas side distributor
- $E_{L,i}$  = relative flow rate deviation in the outlet port  $i$  locating at the third generation of the liquid side distributor
- $E_r$  = relative error between the average liquid side volumetric mass transfer coefficient in parallel microchannels and that in uniform distribution case
- $H$  = height of microchannel, m
- $j$  = superficial velocity, m/s
- $k$  = number of channels occupied by slug or bubbly flow under maldistributed flow case
- $k_L$  = liquid side mass transfer coefficient, m/s
- $k_{LA}$  = liquid side volumetric mass transfer coefficient,  $\text{s}^{-1}$
- $\Delta L$  = length of microchannel, m
- $m$  = mass flow rate, kg/s
- $n$  = number of parallel microchannels
- $n_{GA}$  = number of microchannels occupied by gas alone flow
- $N_i$  = absorption rate of  $\text{CO}_2$  in microchannel  $i$ ,  $\text{mol/s}$
- $n_{\text{ideal}}$  = number of microchannels occupied by the ideal flow pattern
- $n_{LA}$  = number of microchannels occupied by liquid alone flow
- $P_{\text{in}}$  = inlet pressure in the gas feeding line, Pa
- $\Delta P_{\text{fluc}}$  = magnitude of pressure fluctuation, Pa
- $\Delta P_T$  = two-phase total pressure drop, Pa

$s$  = standard deviation between the actual flow rate in parallel microchannels and that under uniform distribution case  
 $U$  = mean velocity of two phases, m/s  
 $W$  = width of microchannel, m

### Dimensionless groups

$Ca$  = capillary number,  $\mu_L U / \sigma$   
 $Re_{GS}$  = superficial gas Reynolds number,  $d_{hjG} \rho_G / \mu_G$   
 $Re_{LS}$  = superficial liquid Reynolds number,  $d_{hjL} \rho_L / \mu_L$   
 $Sc_L$  = liquid-phase Schmidt number,  $\mu_L / (\rho_L D_L)$   
 $We$  = Weber number,  $\rho_L d_{hj} U^2 / \sigma$

### Greek letters

$\alpha, \beta, \gamma, \delta$  = flow distribution parameters in Table 2, dimensionless  
 $\mu$  = viscosity, Pa s  
 $\rho$  = density, kg/m<sup>3</sup>  
 $\nu$  = kinematic viscosity, m<sup>2</sup>/s  
 $\sigma$  = surface tension, N/m

### Subscripts

avg = average  
ch = microchannel  
G = gas phase  
*i* = index of parallel microchannels or the outlet ports in constructal distributors  
L = liquid phase  
PMC = parallel microchannel contactor  
RC = reference contactor  
tot = total  
uni = uniform distribution case

### Literature Cited

- Benson RS, Ponton JW. Process miniaturization—a route to total environmental acceptability? *Chem Eng Res Des.* 1993;71:160–168.
- Charpentier JC. The triplet “molecular processes-product-process” engineering: the future of chemical engineering? *Chem Eng Sci.* 2002;57:4667–4690.
- Ehrfeld W, Hessel V, Löwe H. *Microreactors: New Technology for Modern Chemistry.* Weinheim: Wiley-VCH, 2000.
- Jensen KF. Microreaction engineering—is small better? *Chem Eng Sci.* 2001;56:293–303.
- Gavriilidis A, Angeli P, Cao E, Yeong KK, Wana YSS. Technology and applications of microengineered reactors. *Chem Eng Res Des.* 2002;80:3–30.
- Jähnisch K, Hessel V, Löwe H, Baerns M. Chemistry in microstructured reactors. *Angew Chem Int Ed.* 2004;43:406–446.
- Watts P, Haswell SJ. The application of micro reactors for organic synthesis. *Chem Soc Rev.* 2005;34:235–246.
- TeGrotenhuis WE, Cameron RJ, Viswanathan VV, Wegeng RS. Solvent extraction and gas absorption using microchannel contactors. In: *Proceedings of the Third International Conference on Microreaction Technology.* Berlin-Heidelberg: Springer Verlag, 2000:541–549.
- Yue J, Chen G, Yuan Q, Luo L, Gonthier Y. Hydrodynamics and mass transfer characteristics in gas-liquid flow through a rectangular microchannel. *Chem Eng Sci.* 2007;62:2096–2108.
- Jähnisch K, Baerns M, Hessel V, Ehrfeld W, Haverkamp V, Löwe H, Wille CH, Guber A. Direct fluorination of toluene using elemental fluorine in gas/liquid microreactors. *J Fluorine Chem.* 2000;105:117–128.
- de Mas N, Günther A, Schmidt MA, Jensen KF. Microfabricated multiphase reactors for the selective direct fluorination of aromatics. *Ind Eng Chem Res.* 2003;42:698–710.
- Chambers RD, Fox MA, Holling D, Nakano T, Okazoeb T, Sandford G. Elemental fluorine Part 16. Versatile thin-film gas-liquid multi-channel microreactors for effective scale-out. *Lab Chip.* 2005;5:191–198.
- Wada Y, Schmidt MA, Jensen KF. Flow distribution and ozonolysis in gas-liquid multichannel microreactors. *Ind Eng Chem Res.* 2006;45:8036–8042.
- Leclerc A, Alamé M, Schweich D, Pouteau P, Delattre C, de Bellefon C. Gas-liquid selective oxidations with oxygen under explosive conditions in a micro-structured reactor. *Lab Chip.* 2008;8:814–817.
- Losey MW, Schmidt MA, Jensen KF. Microfabricated multiphase packed-bed reactors: characterization of mass transfer and reactions. *Ind Eng Chem Res.* 2001;40:2555–2562.
- Kobayashi J, Mori Y, Okamoto K, Akiyama R, Ueno M, Kitamori T, Kobayashi S. A microfluidic device for conducting gas-liquid-solid hydrogenation reactions. *Science.* 2004;304:1305–1308.
- Inoue T, Schmidt MA, Jensen KF. Microfabricated multiphase reactors for the direct synthesis of hydrogen peroxide from hydrogen and oxygen. *Ind Eng Chem Res.* 2007;46:1153–1160.
- Wang X, Nie Y, Jasmine LCL, Jaenicke S. Evaluation of multiphase microreactors for the direct formation of hydrogen peroxide. *Appl Catal A.* 2007;317:258–265.
- Hessel V, Angeli P, Gavriilidis A, Löwe H. Gas-liquid and gas-liquid-solid microstructured reactors: contacting principles and applications. *Ind Eng Chem Res.* 2005;44:9750–9769.
- Triplett KA, Ghiaasiaan SM, Abdel-Khalik SI, Sadowski DL. Gas-liquid two-phase flow in microchannels. I. Two-phase flow patterns. *Int J Multiphase Flow.* 1999;25:377–394.
- Chung PMY, Kawaji M. The effect of channel diameter on adiabatic two-phase flow characteristics in microchannels. *Int J Multiphase Flow.* 2004;30:735–761.
- Yue J, Luo L, Gonthier Y, Chen G, Yuan Q. An experimental investigation of gas-liquid two-phase flow in single microchannel contactors. *Chem Eng Sci.* 2008;63:4189–4202.
- Pohorecki R. Effectiveness of interfacial area for mass transfer in two-phase flow in microreactors. *Chem Eng Sci.* 2007;62:6495–6498.
- Yue J, Luo L, Gonthier Y, Chen G, Yuan Q. An experimental study of air-water Taylor flow and mass transfer inside square microchannels. *Chem Eng Sci.* 2009;64:3697–3708.
- Haverkamp V, Emig G, Hessel V, Liauw MA, Löwe H. Characterization of a gas/liquid microreactor, the micro bubble column: determination of specific interfacial area. In: *Proceedings of the Fifth International Conference on Microreaction Technology.* Berlin-Heidelberg: Springer-Verlag, 2002:202–213.
- de Mas N, Günther A, Kraus T, Schmidt MA, Jensen KF. Scale-out multilayer gas-liquid microreactor with integrated velocimetry sensors. *Ind Eng Chem Res.* 2005;44:8997–9013.
- Tondeur D, Luo L. Design and scaling laws of ramified fluid distributors by the constructal approach. *Chem Eng Sci.* 2004;59:1799–1813.
- Bejan A. Constructal theory network of conducting paths for cooling a heat generating volume. *Int J Heat Mass Transfer.* 1997;40:799–811.
- Bejan A, Tondeur D. Equipartition, optimal allocation, and the constructal approach to predicting organization in nature. *Rev Gen Therm.* 1998;37:165–180.
- Bejan A. *Shape and Structure, from Engineering to Nature.* Cambridge, UK: Cambridge University Press, 2000.
- Luo L, Tondeur D, Le Gall H, Corbel S. Constructal approach and multi-scale components. *Appl Therm Eng.* 2007;27:1708–1714.
- Luo L, Fan Y, Zhang W, Yuan X, Midoux N. Integration of constructal distributors to a mini crossflow heat exchanger and their assembly configuration optimization. *Chem Eng Sci.* 2007;62:3605–3619.
- Fan Y, Boichot R, Goldin T, Luo L. Flow distribution property of the constructal distributor and heat transfer intensification in a mini heat exchanger. *AIChE J.* 2008;54:2796–2808.
- Salman W, Gavriilidis A, Angeli P. On the formation of Taylor bubbles in small tubes. *Chem Eng Sci.* 2006;61:6653–6666.
- van Steijn V, Kreutzer MT, Kleijn CR. Velocity fluctuations of segmented flow in microchannels. *Chem Eng J.* 2008;135(Suppl 1):S159–S165.
- Reinecke N, Mewes D. Oscillatory transient two-phase flows in single channels with reference to monolithic catalyst support. *Int J Multiphase Flow.* 1999;25:1373–1393.

37. Günther A, Jensen KF. Multiphase microfluidics: from flow characteristics to chemical and materials synthesis. *Lab Chip*. 2006;6: 1487–1503.
38. Garstecki P, Fuerstman MJ, Stone HA, Whitesides GM. Formation of droplets and bubbles in a microfluidic T-junction—scaling and mechanism of break-up. *Lab Chip*. 2006;6:437–446.
39. van Steijn V, Kreutzer MT, Kleijn CR.  $\mu$ -PIV study of the formation of segmented flow in microfluidic T-junctions. *Chem Eng Sci*. 2007;62:7505–7514.
40. Dufaud O, Le Gall H, Corbel S. Application of stereolithography to chemical engineering ‘from macro to micro’. *Chem Eng Res Des*. 2005;83:133–138.
41. Amador C, Gavriilidis A, Angeli P. Flow distribution in different microreactor scale-out geometries and the effect of manufacturing tolerances and channel blockage. *Chem Eng J*. 2004;101:379–390.
42. Yue J, Chen G, Yuan Q, Luo L, Le Gall H. Mass transfer in gas-liquid flow in microchannels. *J Chem Ind Eng (China)*. 2006;57:1296–1303.

*Manuscript received Mar. 5, 2009, and revision received May 23, 2009.*